



# Benchmarking a 2018 Toyota Camry 2.5-Liter Atkinson Cycle Engine with Cooled-EGR

**John Kargul, Mark Stuhldreher, Daniel Barba, Charles Schenk, Stanislav Bohac, Joseph McDonald, and Paul Dekraker** US Environmental Protection Agency

**Josh Alden** Southwest Research Institute

**Citation:** Kargul, J., Stuhldreher, M., Barba, D., Schenk, C. et al., "Benchmarking a 2018 Toyota Camry 2.5-Liter Atkinson Cycle Engine with Cooled-EGR," SAE Technical Paper 2019-01-0249, 2019, doi:10.4271/2019-01-0249.

## Abstract

**A**s part of the U.S. Environmental Protection Agency's (EPA's) continuing assessment of advanced light-duty automotive technologies in support of regulatory and compliance programs, a 2018 Toyota Camry A25A-FKS 4-cylinder, 2.5-liter, naturally aspirated, Atkinson Cycle engine with cooled exhaust gas recirculation (cEGR) was benchmarked. The engine was tested on an engine dynamometer with and without its 8-speed automatic transmission, and with the engine wiring harness tethered to a complete vehicle parked outside of the test cell. Engine and transmission torque, fuel flow, key engine temperatures and pressures, onboard diagnostics (OBD) data, and Controller Area Network (CAN) bus data were recorded. This paper documents the test results under

idle, low, medium, and high load engine operation. Motoring torque, wide open throttle (WOT) torque and fuel consumption are measured during transient operation using both EPA Tier 2 and Tier 3 test fuels. The design and performance of this 2018 2.5-liter engine is described and compared to Toyota's published data and to EPA's previous projections of the efficiency of an Atkinson Cycle engine with cEGR. The Brake Thermal Efficiency (BTE) map for the Toyota A25A-FKS engine shows a peak efficiency near 40 percent, which is the highest value of any publicly available map for a non-hybrid production gasoline internal combustion (IC) engine designed to run on 91 RON fuel. Further improvement is possible by application of fixed discrete or full continuous cylinder deactivation, both of which are currently in production on other engines.

## Introduction/Background

**T**he National Center for Advanced Technology (NCAT), part of EPA's National Vehicle and Fuel Emissions Laboratory (NVFEL) in Ann Arbor, Michigan, assesses the effectiveness of advanced low emission and low fuel consumption technologies by benchmarking a broad range of key light-duty vehicles, engines and transmissions. The NCAT team benchmarks advanced technologies using laboratory test methods to characterize engine controls, fuel consumption, and emissions [1, 2, 3, 4, 5, 6, 7, 8].

NCAT leverages in-depth, detailed engineering analyses along with extensive engine and chassis dynamometer laboratory testing to evaluate advanced vehicle, engine and transmission technologies. The test data are used for a variety of purposes, including documenting engine performance in complete engine maps, performing technical analyses regarding technology effectiveness, and providing information for full vehicle simulations using EPA's Advanced Light-Duty Powertrain and Hybrid Analysis (ALPHA) tool [9, 10, 11, 12]. Both laboratory test data and ALPHA simulation results support the evaluation of light-duty vehicle fuel economy, greenhouse gas and criteria emissions, and are also being used to evaluate the difference between laboratory and actual in-use emissions.

Atkinson Cycle engines and external cEGR are key technologies being produced today to meet performance targets, greenhouse gas (GHG) and other emissions standards, and fuel economy standards [13, 14].

To understand the current performance and efficiency of these engines, EPA benchmarked a 2018 Toyota Camry equipped with an A25A-FKS 4-cylinder 2.5-liter Atkinson Cycle engine with cEGR and an eight-speed automatic transmission. The complete benchmarking study of this vehicle included both chassis dynamometer testing and engine dynamometer testing to measure vehicle and engine efficiencies. The paper focuses on the following aspects of the benchmarking study:

1. *Engine Benchmarking Methods* - The benchmark testing involved installing the engine in an engine dynamometer test cell with the engine wiring harness tethered to the complete vehicle parked outside the test cell. This technique enabled the engine to be mapped using the vehicle's original equipment engine control unit (ECU) with its as-built calibrations along with all the needed input signals, including those integrated with other vehicle sensors. This section of the paper reviews EPA's methods to collect engine data such as torque, fuel flow,

temperatures, pressures, crankshaft and camshaft positioning, and onboard diagnostics (OBD)/Controller Area Network (CAN) bus data collection, as described in more detail in [1]. In addition, new methods used by EPA to accurately measure valve timing and cEGR are presented.

2. *Test Data Analysis* - Engine data were collected using both steady-state and transient test procedures to appropriately characterize engine operation at idle, low-, mid-, and high- loads. At the higher loads, a transient test procedure was used to observe the changing control and performance of the engine that often occurs when the ECU begins to protect the engine from excessive temperatures, pre-ignition and knock. Again, more detailed descriptions of these test data analysis methods and techniques were provided in [1].
3. *Fuel Consumption Maps* - After the engine benchmark data collection was completed, engine fuel efficiency maps suitable for modeling and simulation were generated from the engine test data. These maps are needed as inputs to ALPHA, EPA's full vehicle simulation model, to estimate carbon dioxide ( $\text{CO}_2$ ) emissions over the regulatory city and highway drive cycles. To simulate drive cycle performance, the ALPHA model requires various vehicle parameters as inputs, including vehicle inertia and road load coefficients, component efficiencies, and vehicle operational data [10].
4. *Comparison to Toyota's Published Fuel Consumption Map* - The fuel consumption map generated from benchmark testing was compared against the fuel consumption map for the same engine published by Toyota [13].
5. *Comparison to EPA's Previous Efforts to Model and Validate a Future Atkinson Engine with cEGR* - The EPA benchmark results for the Toyota 2.5-liter A25A-FKS engine were compared to previous data from EPA's GT-POWER modeling and test cell validation demonstration of an Atkinson Cycle engine with cEGR [15, 16].
6. *Potential for Improving Efficiency* - Finally, estimates of the effectiveness of adding cylinder deactivation to the A25A-FKS engine for additional  $\text{CO}_2$  reduction are discussed.

## 1. Engine Benchmarking Methods

EPA's method for benchmarking an engine involved installing the engine in an engine dynamometer test cell while connecting (tethering) the engine's wiring harness to the complete vehicle, which is parked adjacent to the test cell as shown in Figure 1. This technique enables the engine to be operated using the vehicle's original equipment (OE) engine control unit (ECU) with its as-built calibrations along with all the needed input signals, including those integrated with other vehicle sensors. Additional details of EPA's

**FIGURE 1** Engine dynamometer and tethered vehicle installation.



2019 US Environmental Protection Agency.

benchmarking and analysis methodologies are contained in several previous papers [1, 2, 3, 4, 5, 6, 7].

## Description of Test Article

The engine used in this project was a 2018 Toyota Camry 2.5-liter A25A-FKS engine, which is a naturally aspirated, Atkinson Cycle, spark-ignition gasoline engine [14, 15]. The engine uses port and side direct fuel injection systems (PFI/GDI, referred to by Toyota as D-4S); a cooled, external exhaust gas recirculation system (cEGR); and a wide range of authority variable valve timing with electric phasing on the intake camshaft and hydraulic phasing on the exhaust camshaft. Atkinson Cycle is implemented using late intake valve closing (LIVC). Effective compression ratio is varied by varying intake camshaft phasing. The A25A-FKS engine is used as the base engine in non-hybrid Toyota light-duty vehicle applications (e.g., Camry [37], RAV4 [38]), while the similar A25A-FXS engine is specifically calibrated for use in hybrid electric vehicle applications (e.g., Camry Hybrid [37], Avalon Hybrid [39], RAV4 Hybrid [38]). A comparable 2.0L inline 4-cylinder (I4) Atkinson Cycle engine with cEGR, the M20A-FKS, is also used as the base engine for U.S.-market versions of the 2019 Toyota Corolla [40]. Table 1 summarizes information that identifies vehicle system used in this test program.

## Test Site

Testing was performed in a light-duty engine dynamometer test cell located at the National Vehicle and Fuel Emissions Laboratory (NVFEL) in Ann Arbor, Michigan. The test cell equipment and instrumentation are listed in Table 2.

## Data Collection Systems

Test cell data acquisition and dynamometer control were performed by iTesT, a software package developed by A&D Technology, Inc., and an MTS Combustion Analysis System

## BENCHMARKING A 2018 TOYOTA CAMRY 2.5-LITER ATKINSON CYCLE ENGINE WITH COOLED-EGR

(CAS) was used to verify that the engine was operating correctly. RPECS-IV (Rapid Prototyping Electronic Control System - IV) is supplemental data acquisition software developed by Southwest Research Institute (SwRI). RPECS directly measures and logs ECU input/output (I/O) along with test cell data. Temperatures, pressures, and test cell data were sent

**TABLE 1** Vehicle and Engine Identification Information [13, 14]

Vehicle (Year, Make, Model)	2018 Toyota Camry LE
Vehicle Identification Number	JTNB11HKXJ3007695
Emissions Test Group	JTYXV02.5P3A
Engine (displacement, name)	2.5-liter, A25A-FKS "Dynamic Force"
Rated Power	151 kW @ 6600 RPM
Rated Torque	249 Nm @ 4800 RPM
Geometric Compression Ratio (approximate expansion ratio)	13:1
Crankshaft offset	10.1 mm
Stroke/Bore Ratio	1.2
Fuel requirement	87 octane Anti-Knock Index (AKI)
Emission level	Federal Tier 3 Bin 30/California LEV-III SULEV30
Advanced engine technology features (based on Toyota's publicly released information)	<ul style="list-style-type: none"> <li>• Direct Injection &amp; Port Injection</li> <li>• Atkinson Cycle</li> <li>• Cooled EGR</li> <li>• VVT Electric Intake/Hydraulic Exhaust</li> <li>• High induction turbulence/high speed combustion</li> <li>• Variable capacity oil pump</li> <li>• Electric water pump</li> <li>• High energy ignition</li> <li>• Friction reduction</li> </ul>
Transmission	Eight-speed automatic transmission

2019 US Environmental Protection Agency.

**TABLE 2** Test Cell Equipment and Instrumentation

Equipment/Instrument Name	Purpose/Measurement Capabilities	Manufacturer
Dynamometer (Alternating Current)	Absorb torque from engine and provide motoring torque to engine	Meidensha Corp., Tokyo, Japan
Torque Sensor	Measure torque	HBM GmbH, Darmstadt, Germany
CVS dilution tunnel	Exhaust flow system	EPA
Coriolis fuel meter	Measure Fuel flow rate	Emerson Micro Motion, St. Louis, MO
Laminar flow element	Measure Air flow rate	Meriam Process Technologies, Cleveland, OH

2019 US Environmental Protection Agency.

from iTest to RPECS via CAN. The engine control and analysis systems are summarized in [Table 3](#).

## Engine Configuration

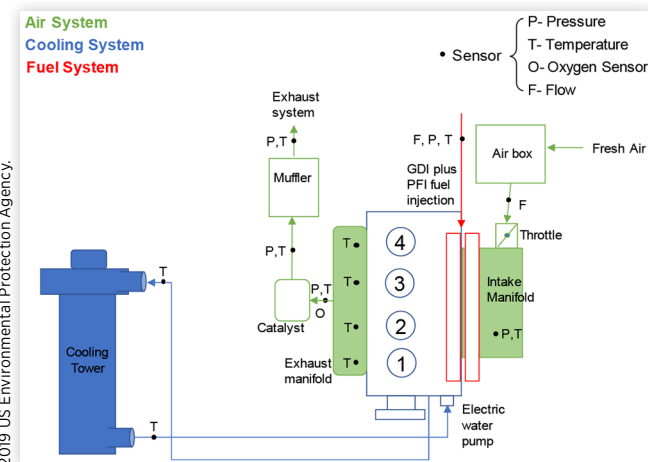
[Figure 2](#) illustrates the engine configuration and sensor location in the dynamometer test cell. The sensor colors shown in the upper left corner of the figure indicate which systems are monitored.

The OE engine systems were used with the addition of instrumentation as follows:

- *Intake:* The OE air box and plumbing were used.
- *Exhaust:* The OE exhaust system was used including catalyst and mufflers. The exhaust system outlet was connected to the constant volume sampling system (CVS) dilution tunnel via 2-inch diameter tubing.

**TABLE 3** Engine Control and Data Acquisition Systems

System	Developer	Description	Data Rate
iTest	A&D Technology, Inc., Ann Arbor, MI	Test cell automation hardware and software system that controls the dynamometer and some engine controls; collects test cell data; master data logger.	10-100 Hz
MATLAB	MathWorks, Natick, MA	Software used for development of data processing algorithms for transient testing	--
RPECS	Southwest Research Institute, San Antonio, TX	Crank angle-based engine control and data acquisition system that collects ECU analog and CAN data, TCU analog and CAN data, and controls torque converter lock up solenoid.	1/engine cycle

**FIGURE 2** Schematic of dynamometer test cell and the A25A-FKS engine sensor locations corresponding to the identified systems

2019 US Environmental Protection Agency.

CVS pressure was controlled to approximately  $P_{atm} \pm 1.2 \text{ kPa}$ , which is a variation of pressure well below the required limits specified within the U.S. Code of Federal Regulations for chassis dynamometer testing [17].

- *Cooling system:* The OE cooling system was used, but the radiator was replaced with a cooling tower. The OE engine thermostat and electric water pump were used to control engine coolant temperature. The cooling tower was controlled to 85°C by the test cell control system.
- *Oil system:* The engine oil was cooled by adding a sandwich oil filter manifold which allows oil to be routed to an external heat exchanger. This heat exchanger was connected to a chilled water system and controlled to 90°C by the test cell control system.
- *Front End Accessory Drive (FEAD):* The OE serpentine belt was removed for this testing. The water pump was electrically driven and controlled by the ECU. Any losses associated with the FEAD were not included in the final Brake Specific Fuel Consumption (BSFC) or Brake Thermal Efficiency (BTE) maps.
- *Alternator:* No alternator was used.
- *Fuel:* The engine tests were performed with the EPA Certification Tier 2 and Tier 3 fuels shown in [Table 4](#).

## Valve Timing Measurement

Nearly all engines (approximately 98.8 percent in model year 2017) for light-duty vehicle applications in the U.S. are equipped with variable valve timing (VVT) [18]. VVT enables control of many aspects of air flow, exhaust scavenging, and combustion relative to fixed valve timing engines. Engine parameters such as volumetric efficiency, effective compression ratio, and internal exhaust gas recirculation (EGR) can all be controlled by the VVT system. When testing, the precise intake and exhaust valve opening and closing, must be known to calculate and understand these parameters. A method was developed to measure the valve lift and timing under actual engine operation with active VVT control and with a pressurized oil system. This method is non-intrusive, accurate, and can be accomplished in a reasonable amount of time.

**TABLE 4** Test Cell Fuel Specifications

	EPA Tier 2 Certification Fuel	EPA Tier 3 Certification Fuel
Fuel Grade	Premium	Regular
Ethanol Content (% vol.) ASTM D5599	0%	10%
Lower Heating Value (LHV) (MJ/kg) ASTM D240	42.91	41.95
Specific Gravity@60°F ASTM D4052	0.74320	0.74400
Carbon Weight Fraction ASTM D3343	0.86633	0.8299

2019 US Environmental Protection Agency.

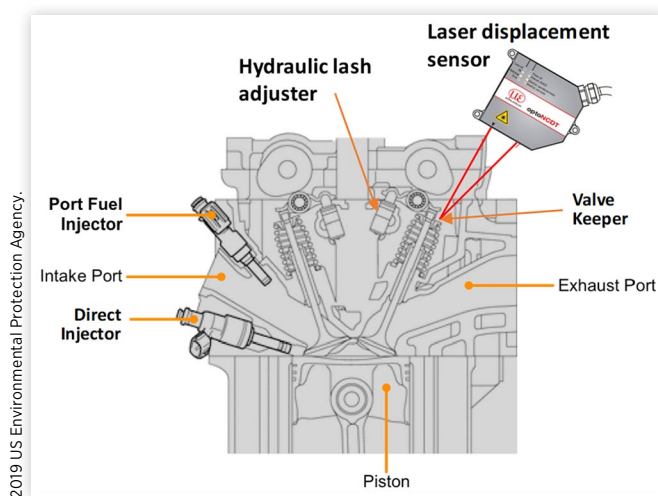
**Methods Considered to Measure Valve Lift:** This section describes how to precisely measure valve lift for both the intake and exhaust valves in the crank angle domain. For this study, valve lift is determined by measuring the valve's opening, closing and camshaft phase during engine operation. Several methods were considered as noted below. The first three methods were not chosen due to challenges noted.

1. *Measurement with dial indicator and degree wheel -* This method mounts a degree wheel on the crankshaft and dial indicator on the valve keeper. The crankshaft is rotated by hand and the dial indicator reading is recorded for each crank angle. This method is fairly accurate but has difficulties such as the degree wheel mounting, hydraulic valve lash adjusters collapsing without oil pressure, crankshaft not rotating smoothly through the entire cycle, and the electric camshaft phaser position is unknown.
2. *Instrumentation of the cylinder head to measure valve displacement -* One type of instrumentation for this method would be to use inductive sensors. This requires the cylinder head to be removed and machined for sensor installation, which could be prohibitively expensive.
3. *Using manufacturer supplied camshaft timing information -* The manufacturer's service manuals sometimes have valve timing information, but these often lack necessary details such as lift measurement and phase angle.
4. *Measurement with laser displacement sensor while cranking engine (the method selected for this study) -* The setup involves removing the valve cover and mounting the laser sensor in clear line of sight to the top of the valve keeper. This method did not require any special adaptations to the cylinder head. The test is conducted by cranking the engine with the starter and measuring the valve lift (from the recorded motion of the valve keeper), camshaft, and crankshaft sensor signals.

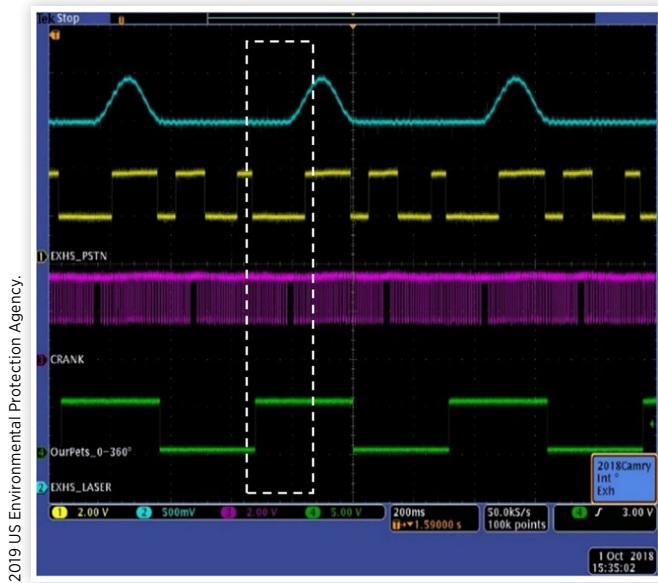
**Capture of Valve Lift Data:** The laser measurement method uses the instrumentation setup shown in [Figure 3](#), while the engine is cranked rather than running at idle, otherwise normal engine lubrication can create an oil spray, or oil film on the keeper, both of which will interfere with the laser signal. Cranking the engine with the starter motor supplies enough oil pressure to fill the hydraulic valve lash adjusters but not to enough to spray oil over the valve keeper. During the cranking for this test the camshaft phase angle was held fixed by the ECU. The camshaft phase angle was measured independent of the ECU along with the laser displacement sensor readings to determine the valve lift profile.

The analog output of the laser displacement sensor was recorded alongside the digital outputs of the camshaft position (CMP) sensor and crank position (CKP) sensor on an oscilloscope during engine cranking as shown in [Figure 4](#). The signal trace data acquired by the oscilloscope were saved to a data file for post-processing. The blue trace in [Figure 4](#) represents the valve lift (the laser signal), the yellow trace is the CMP, the purple trace is the CKP, the green trace shows a reference for TDC of cylinder 1. These measurements were

## BENCHMARKING A 2018 TOYOTA CAMRY 2.5-LITER ATKINSON CYCLE ENGINE WITH COOLED-EGR

**FIGURE 3** Cylinder head valve train and laser sensor.

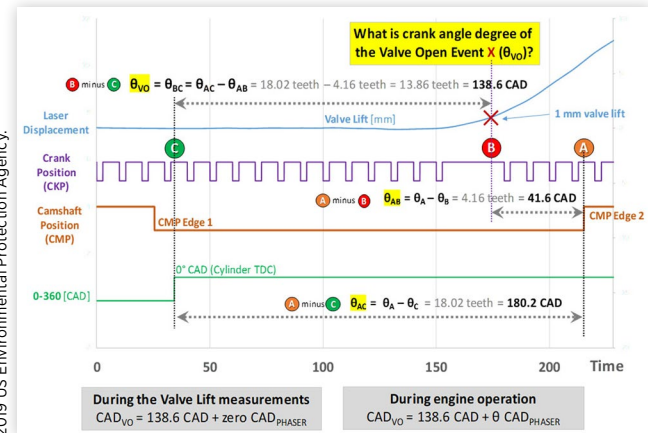
2019 US Environmental Protection Agency.

**FIGURE 4** Representative oscilloscope screen capture of laser displacement sensor signals used to measure valve lift, as well as the CMP and CKP data.

performed for both the intake and the exhaust valve for cylinder 1 and then phased for the other cylinders.

**Data analysis of the captured data:** Figure 5 represents an expanded plot of a short time segment from within the dashed white rectangle visible on the captured oscilloscope data in Figure 4. The graph in Figure 5 shows the valve lift data captured from the laser sensor. The crank teeth are shown as measured by the CKP. The 0-360 signal shows when top dead center for the cylinder occurred with the camshaft phaser in the “zero” phase position. For this engine “zero” camshaft phase was defined such that it matched what the OE ECU reports over onboard diagnostics (OBD). Finally, the camshaft position sensor reveals two of the cam encoder tooth edges, labeled as CMP Edge 1 and CMP Edge 2.

The amount of valve lift is measured by the laser displacement sensor. However, to determine the actual crank angle of

**FIGURE 5** Analysis of a time slice of the captured valve lift data with “zero” camshaft phase.

a valve lift event with respect to TDC (difference in degrees between points B and C in Figure 5), one must:

1. **Determine location of 1 mm Valve Lift Event X relative to a reference cam encoder tooth edge** (called  $\theta_{AB}$  as the difference in degrees between points A and B in Figure 5)

Valve opening (or closing) events were defined as 1 mm of lift and located within the filtered signal as shown in Figure 5 as a red 'X'. The key principle here is to measure the offset of valve lift event relative to closest edge of a camshaft encoder tooth on the camshaft. Since the camshaft encoder is mechanically fixed relative to the camshaft lobes, the relative angle from valve open (or close) event (labeled with a B in a red circle in Figure 5) to the CMP rising (or falling) signal edge (labeled with an A in an orange circle in Figure 5) is constant. To determine this constant offset, the valve lift data was first filtered using the Savitzky-Golay method.

From these event locations, the nearest edge of the CMP signal (CMP Edge 2 in Figure 5) was selected. The offset from the valve event to the nearest CMP signal edge could then be measured (Figure 5, shortest dotted arrow from points A to B) using the signal recorded synchronously from the crankshaft position sensor.

Having a crankshaft position encoder with a typical 36-tooth pattern, the number of full and fractional pulses was counted from valve event to selected edge of the CMP signal, then multiplied by 10-CAD/pulse. This calculation method results in offset between valve event and camshaft encoder with minimal error utilizing the OE crankshaft encoder. A potential refinement of this method would use a higher resolution encoder installed on the crankshaft, but such a refinement would incur additional cost.

2. **Determine location of cam encoder tooth edge relative to TDC** (called  $\theta_{AC}$  as the difference in degrees between points A and C in Figure 5 with no camshaft phasing)

For the offset between the CMP encoder edge and the valve event to be meaningful, the position of the CMP encoder edges must be known relative to cylinder TDC (Figure 5, dotted arrow from points B to C).

$\theta_{AC}$  will change as the VVT cam phaser is actuated, thus it is important that a reference measurement is made at a known phase measurement. The reference phase can be at any arbitrary angle, or at a physical stop at either end of travel. However, this reference phase measurement must be utilized when calculating valve timing or an offset will be generated in the results. The sign of phase measurements must also be considered in this context as the absolute phase measurements for intake and exhaust cams are normally in opposite directions.  $\theta_{BC}$  can be split into 3 terms,  $\theta_{BC@ref}$  the measurement of  $\theta_{BC}$  at the reference cam phase point,  $\theta_{phase@ref}$  the assumed phasing quantity at the reference cam phase point, and  $\theta_{phase}$  the relative phasing applied at a given point.

For this measurement effort, the reference angle of zero camshaft phase was chosen to match that as reported over the vehicle's OBD. Furthermore, the OBD tool used for this measurement effort allowed for overriding the camshaft phaser control, forcing the camshafts to zero phase as reported by OBD.

### 3. Determine the location of valve opening (or closing event) with respect to TDC for a given cam phase:

Finally, to determine the valve event location relative to cylinder TDC ( $\theta_{BC}$ ) the measurement of  $\theta_{AB}$  can be subtracted from the measurement of  $\theta_{AC}$ . Knowing that  $\theta_{AB}$  is constant and  $\theta_{AC}$  can be split, yields the equations (1) that provide the reference to determine the valve event location during normal operation from the phase measurement, as shown in Figure 5.

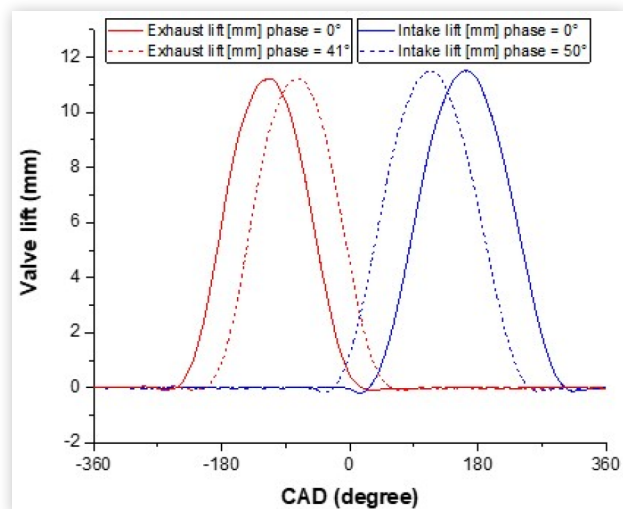
$$\begin{aligned} \theta_{VO} &= \theta_{BC} \\ &= \theta_{AC} - \theta_{AB} \\ &= (\theta_{AC@ref} + \theta_{phase} - \theta_{phase@ref}) - \theta_{AB} \\ &= (18.02 + 0 - 0) - 4.16 \text{ teeth} \\ &= 13.86 \text{ teeth} + \theta_{phase} \quad \text{or} \\ &= 138.6 \text{ CAD} + \theta_{phase} \end{aligned} \quad (1)$$

**Final valve lift profile:** The raw valve lift and sensor signals were recorded on an oscilloscope in time domain. The results were post processed to convert to crank angle domain and valve lift in mm. Figure 6 shows the intake and exhaust valve lift at zero and max phase angle CAD. Valve timings such as intake valve open (IVO), intake valve close (IVC), exhaust valve open (EVO), and exhaust valve close (EVC) can be calculated at 1 mm lift. The engine maps with measured phase angle can then be converted to actual IVO, IVC, EVO, and EVC which then can be used to calculate valve overlap Atkinson Ratio (effective expansion ratio/effective compression ratio), and actual compression ratios.

## Cooled EGR Measurement

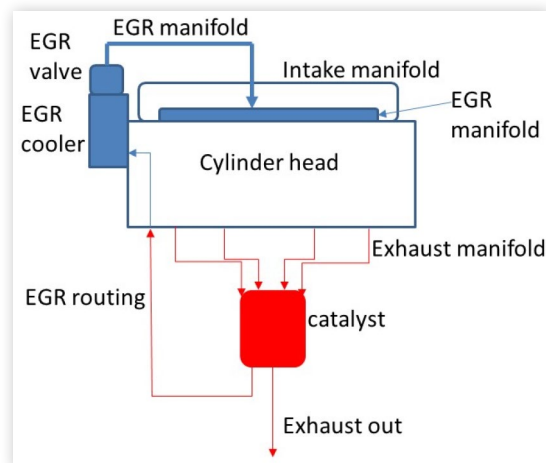
Toyota's cEGR technology is used on this engine to improve thermal efficiency, reduce pumping work and suppress knock [19]. Figure 7 shows the configuration and routing of the

**FIGURE 6** Intake and exhaust valve lift profile from laser displacement sensor.



2019 US Environmental Protection Agency.

**FIGURE 7** Toyota 2.5L A25A-FKS engine EGR system and routing.



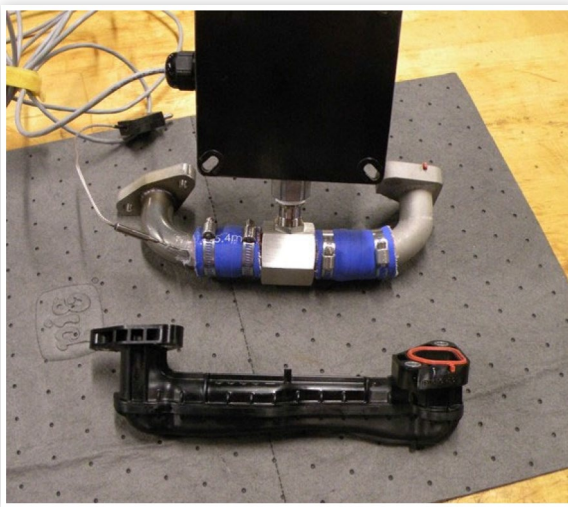
2019 US Environmental Protection Agency.

engine's EGR system. Measuring the amount of EGR requires special instrumentation and test methods.

**cEGR Measurement Method:** The method used to measure the amount of EGR flow through the cEGR system was to replace the EGR manifold (connecting the EGR valve to intake manifold) with the fabricated manifold containing the flow meter and thermocouple shown in Figures 8 and 9. The system was designed so the OE EGR manifold could be unbolted, and the fabricated manifold bolted directly in place. Special care was taken when designing the instrumented manifold to mimic the flow of the OE manifold. The flowmeter used was a turbine flowmeter calibrated for air with a thermocouple on the outlet of the flowmeter.

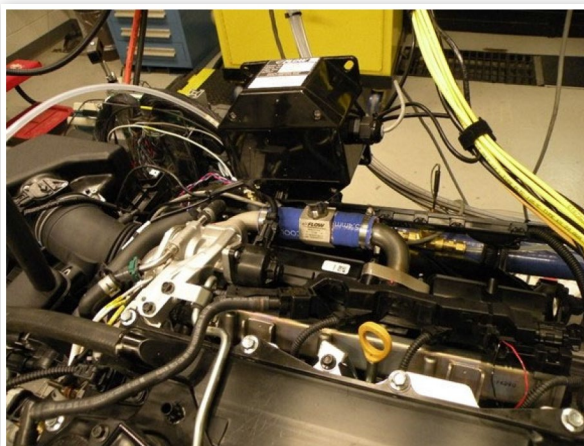
**EGR calculations:** The external EGR flow was measured directly by the flow meter in actual cubic feet per minute (ACFM). This was converted to standard cubic feet per minute (SCFM) using the intake manifold pressure and EGR temperature at the flowmeter exit. This flow and the intake air flow,

**FIGURE 8** OE EGR manifold (bottom of photo) vs fabricated/instrumented manifold (middle of photo).



2019 US Environmental Protection Agency.

**FIGURE 9** Fabricated/instrumented manifold with flow meter mounted on engine.



measured by mass air flow sensor, were used to calculate the percent EGR by volume.

The test to determine the EGR flows was conducted as a separate test from the standard steady-state benchmarking testing. The test consisted of running the engine and logging data using the steady state method. The number of sampling points were abbreviated from the standard steady state tests and conducted only under conditions where the ECU opened the EGR valve.

The influence of the fabricated manifold and flowmeter on the operation of the engine was considered negligible. Data from both steady state and this EGR flow test were compared and there was no significant difference in how the engine operated, including spark timing, intake manifold temperature, mass air flow and thermal efficiency. A fuel flow data comparison with and without the fabricated manifold revealed that fuel consumption was 1 to 2 percent higher for the tests with the fabricated EGR manifold with about half of this within test-to-test variability. The tests with the fabricated

manifold were only used to study the amount of cooled external EGR implemented in Toyota's A25A-FKS engine.

## Engine-Dynamometer Setup

To gather data for this benchmarking program, the engine was connected to the dynamometer via a GM 6L80 6-speed rear drive automatic transmission and torque converter, and drive shaft as shown in Figures 10 and 11. This transmission has been setup by EPA for general use in engine benchmark testing. There are several reasons an automatic transmission was used.

1. Minimize torsional vibrations. The transmission and torque converter have built in torsional damping. This allows low speed and high torque testing that could not be done with just a driveshaft connection.
2. The transmission is easily adapted to any engine.
3. The transmission gears selection and torque converter clutch are manually controlled. The gear ratios in overdrive allow a higher torque engine to be tested.

**FIGURE 10** Engine and Transmission Setup with Torque Sensors.

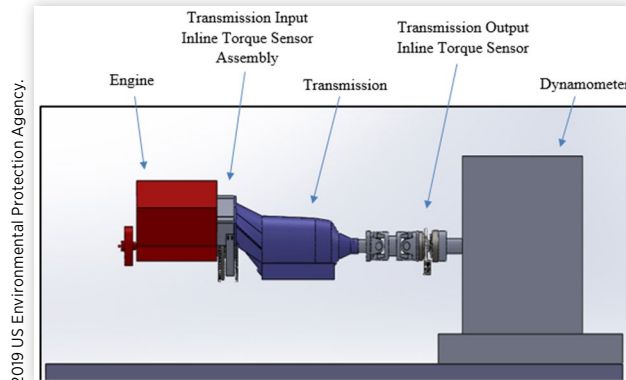


**FIGURE 11** Engine and GM 6L80 automatic transmission setup in the test cell.



2019 US Environmental Protection Agency.

4. The transmission can be placed in neutral to allow idling and unloaded operation.
5. The transmission enables starting the engine with a production starter, which is important when doing cold start testing.

The GM6L80 6-speed transmission has the load capacity for the test cell dyno and is easily adapted to any engine configuration. This engine setup allowed data to be gathered throughout the complete speed range including low speed with no driveline resonance. This transmission setup enabled the ability to gather data at idle to compute engine idle fuel consumption. The engine could also be started normally with the engine starter to replicate the starting behavior as installed in the vehicle. The engine could also operate at idle and low speeds with normal transmission loading and an unlocked torque converter. More complete details of this test and setup have been previously described [9].

## 2. Test Data Analysis

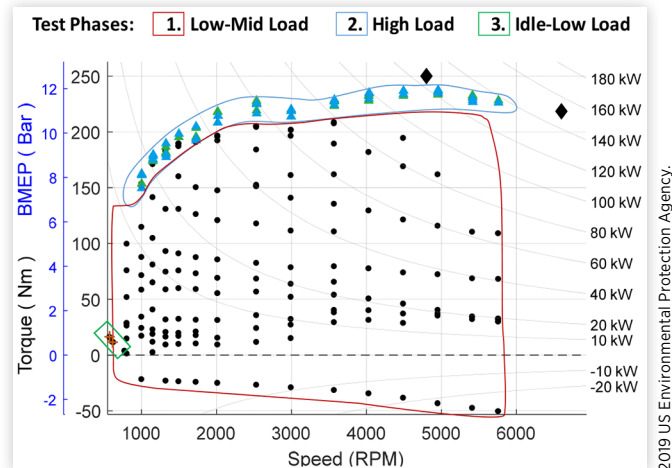
Steady-state, transient and idle engine test data were collected during the benchmark testing. Different test procedures were needed to appropriately replicate the engine operation and engine management system calibration for idle, part load conditions, and at high load conditions nearing peak brake mean effective pressure (BMEP). Detailed descriptions of the data collected, the calculation, and the analytical methodologies used to analyze the datasets on the Toyota A25A-FKS engine were very similar to those used for previous EPA testing of the 2016 Honda Civic 1.5-liter L15B7 turbocharged engine [1].

The data collected from the Toyota engine were analyzed to generate brake specific fuel consumption (BSFC), brake thermal efficiency (BTE), exhaust lambda, compression ratio, exhaust camshaft phasing, intake camshaft phasing, Atkinson Ratio (effective expansion ratio/effective compression ratio), spark timing, and valve overlap charts which can be viewed in the Appendix. The remaining part of this section will highlight some of the notable observations from the Toyota engine.

**Engine Mapping Test Data Points:** Figure 12 shows steady-state, low speed/low load, and transient data points gathered from the A25A-FKS engine. The steady state test points were gathered with the automatic transmission held in 4<sup>th</sup> gear and are an average of 10 Hz data over a 10 second window after stable consistent engine control was observed (e.g. spark timing, valve timing, start of injection). Low speed near idle data points were obtained with the automatic transmission held in neutral.

For each transient test point, the accelerator pedal was held at about 1/3 load and the engine was allowed to stabilize. The accelerator pedal was then ramped from 1/3 load to the specified high load in one second. For each data point, the data are logged continuously at 100 Hz while the engine torque ramped up to the desired torque value and while operation was held at that point for 30 seconds. The data were then post-processed to determine the peak torque, final torque,

**FIGURE 12** Engine Mapping Test Data Points from benchmarking 2018 Toyota 2.5L A25A-FKS engine using Tier 2 test fuel.



2019 US Environmental Protection Agency.

### Legend for Engine Maps like Figure 12\*

- Core Map Steady-State Operating Points  
(engine coupled to dynamometer through an automatic transmission held in 4<sup>th</sup> gear)
- ✚ Low Speed/Near Idle Steady-State Operating Points  
(engine coupled to transmission held in neutral)
- ▲ High Load Transient Operating Points - Initial Value
- ▲ High Load Transient Operating Points - Final Value
- ◆ Maximum torque points (from published data [13, 14])

\*Note: This legend applies to engine maps throughout the paper.

2019 US Environmental Protection Agency.

transition time from stoichiometric to commanded fuel enrichment (could be essentially instantaneous), BTE, and other key engine criteria.

To characterize the transient nature of the high load region of operation, an “initial” time window after the target high load torque is achieved was identified, as well as a “final” time window after control stabilizes to a long term steady state value. A graphic example of a transient data set for the Toyota A25A-FKS engine is shown in Figure 13. Data over these windows were averaged and used to complete the engine map as shown in Figure 12.

It should be noted that initial and final values for the Toyota A25A-FKS are remarkably similar to each other, as compared to the Honda L15B7 turbocharged engine recently benchmarked by EPA using the same high load transient test method. For the Honda engine, wider variation between initial and final test values were observed [1]. For example, Figure 14 shows a comparison of initial and final exhaust lambda maps for the Toyota A25A-FKS engine, which are nearly identical in the high load transient region of operation. The Appendix contains more examples of initial and final test data.

**Injector Fuel Flow Correlation:** To determine fuel consumption during high-load transient operation, data from

## BENCHMARKING A 2018 TOYOTA CAMRY 2.5-LITER ATKINSON CYCLE ENGINE WITH COOLED-EGR

**FIGURE 13** Example high load test conducted on Toyota A25A-FKS engine showing several pertinent parameters and the windows of data selected.

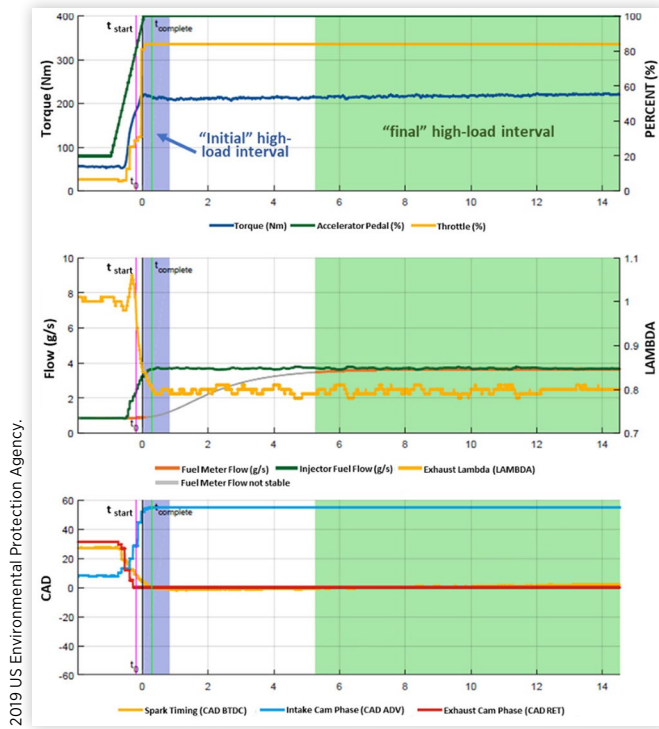
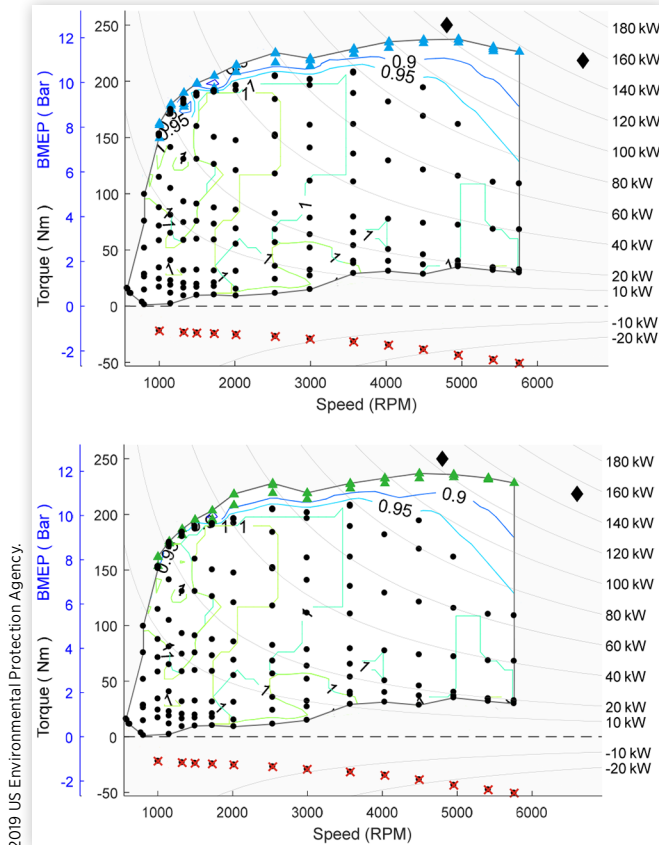


**FIGURE 14** Toyota A25A-FKS engine's average exhaust lambda in the initial (top chart) and final (bottom chart) intervals of the transient high load data, on Tier 2 fuel.



2019 US Environmental Protection Agency.

fuel injectors was used so that quick changes in fueling were accurately captured. The Toyota A25A-FKS engine utilizes both port fuel injection (PFI) and gasoline direct injection (GDI) systems. Toyota refers to the system as “D-4S” and states that it uses both direct injection (DI) and port fuel injection (PFI) injection methods together and interchangeably to optimize engine performance and emissions [21].

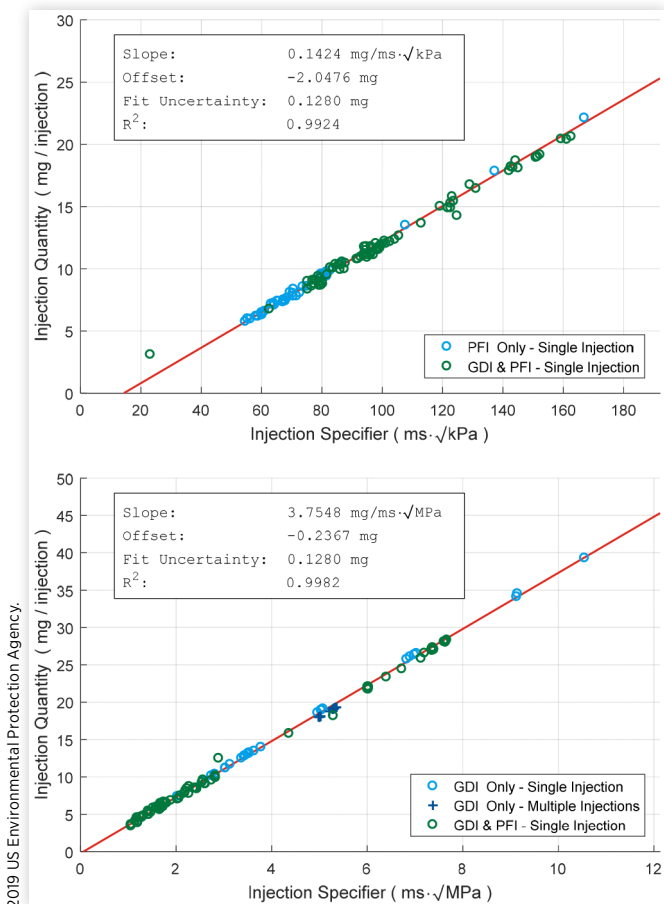
Both the PFI and GDI fuel injectors were calibrated to determine the relationship between injection pulse width and fuel consumption during high-load transient testing. Figure 15 shows the resulting calibration data.

Both PFI and GDI fuel injectors systems are used at low loads, while only GDI is used at high load. This is consistent with Toyota’s previous description of their 4-DS multi hole DI+PFI fuel injection [28]. Figure 16 shows the percentage of PFI (%) used across the engine map. Detailed maps showing both the PFI and GDI fuel flow are shown in the Appendix.

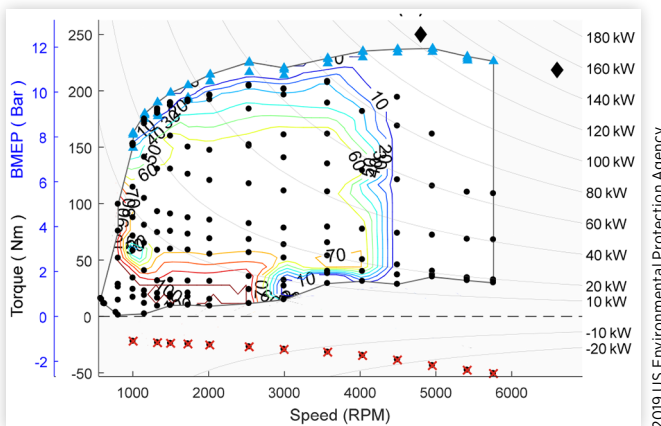
**Cooled Exhaust Gas Recirculation:** Figure 17 shows the ECM’s targeted percent opening of the EGR valve in the A25A-FKS engine, as recorded during the benchmarking of the engine.

Figure 18 shows the percent volume of EGR in the intake charge, as measured using the fabricated EGR manifold shown in Figure 8. At approximately 1750 rpm and 150 Nm the A25A-FKS uses over 24 percent EGR in the intake charge. This compares well with the 25 percent maximum EGR limit

**FIGURE 15** Injector Calibration Data (top chart is for the PFI system, bottom chart is for the GDI system).



**FIGURE 16** Percent portion of fuel supplied by PFI in the Toyota A25A-FKS engine, on Tier 2 fuel (initial interval).



**FIGURE 17** ECM's targeted percent opening of the EGR valve in the A25A-FKS engine, on Tier 2 fuel, (initial interval).

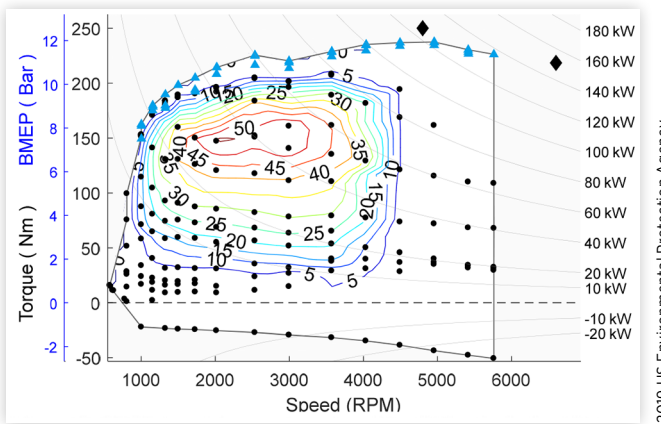
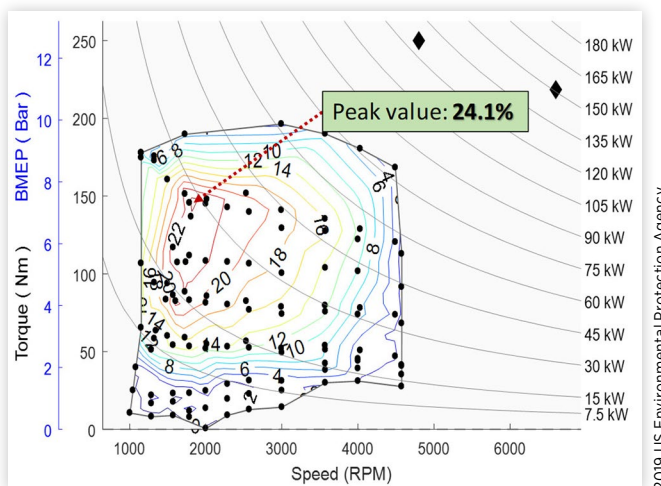


**FIGURE 18** Percent volume of EGR as reported by EPA test cell measurements of the A25A-FKS engine using the fabricated cEGR manifold shown in Figure 8, on Tier 2 fuel.



described by Toyota [19] and is comparable to the 22 percent peak EGR rate achieved by EPA during its Atkinson Cycle/cEGR developmental testing [16].

**Valve Timing:** The charts related to valve timing are derived from valve measurements described earlier in the “Valve Timing Measurement” section of this paper and are based on valve event measurements at 1 mm lift. The effective expansion ratio, effective compression ratio, and Atkinson Ratio maps shown in Figures 19, 20, and 22, respectively, help characterize valve timing operation in the Toyota A25A-FKS engine.

The effective expansion ratio map shown in Figure 19 indicates that exhaust valve timing changes very little over the entire operating map (ratio varies between 12.5:1 and 13.05:1). In contrast, the effective compression ratio map in Figure 20 indicates that intake valve timing varies significantly over the entire operating map (ratio varies between 7:1 to over 11:1). This is expected, since the Toyota engine accomplishes Atkinson Cycle through Late Intake Valve Closing (LIVC) and uses a fast, wide authority electrically-actuated intake camshaft phaser.

Significant use of LIVC can be seen in the low- and mid-load area of the map shown in Figure 20 where the

**FIGURE 19** Effective Expansion Ratio in the A25A-FKS engine, on Tier 2 fuel, 1 mm reference lift, (initial interval).

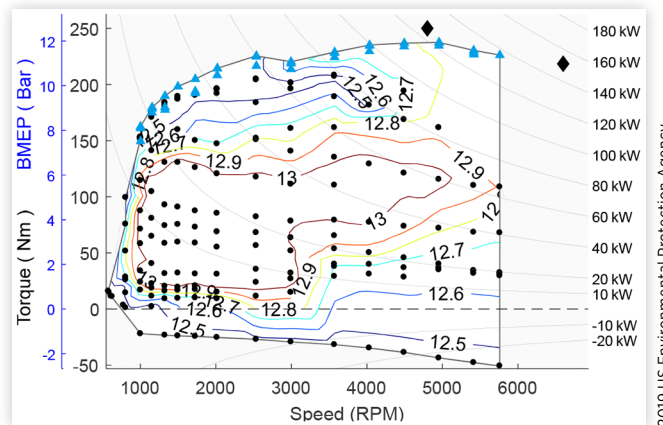
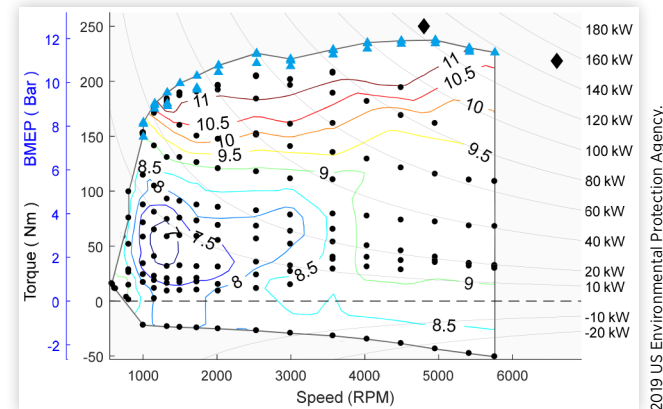


**FIGURE 20** Effective Compression Ratio in the A25A-FKS engine, on Tier 2 fuel, 1 mm reference lift, (initial interval).



effective compression ratio is reduced to as low as 7:1. By controlling airflow via camshaft phasing rather than using the throttle valve, Toyota reduces part-load pumping losses, thereby increasing engine efficiency during low- and mid-load, low speed conditions.

A similar approach was observed during previous EPA benchmark testing of the Mazda 2.0L 13:1 geometric compression ratio (CR) SKYACTIV-G engine [4], which also used Atkinson Cycle and an electrically actuated intake camshaft phaser, but without cEGR as shown in Figure 21.

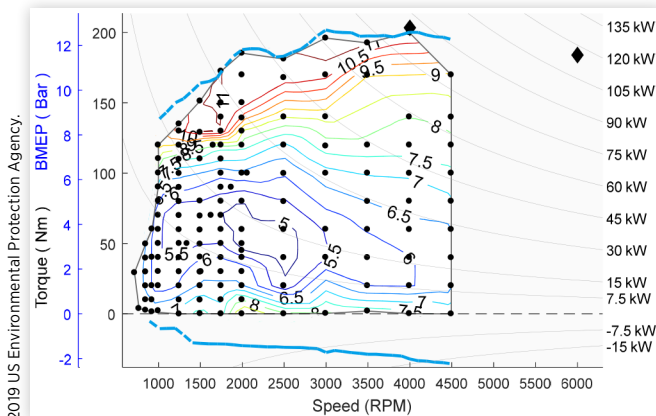
The effective compression ratio is lower for the Mazda engine (5:1 for the Mazda engine in Figure 21 as compared to 7:1 for the Toyota engine in the Figure 20), although it should be noted that the Toyota engine also displaces some intake charge with cEGR under comparable conditions.

Atkinson Ratio (or degree of Atkinson cycle utilization) is another useful way to compare the valve timing of engines. Atkinson Ratio is defined as the effective compression ratio divided by the effective expansion ratio. Atkinson Ratio for the Toyota A25A-FKS engine (Figure 22) peaks at about 2.1 at 1300 rpm and 60 Nm, compared to the Atkinson Ratio for the Mazda (Figure 23) which peaks at 3.2 at 2250 rpm and 50 Nm. In contrast, a non-Atkinson naturally aspirated engine like a GM 2.5L EcoTec engine would have Atkinson Ratio near 1 across the entire map.

While the Toyota uses less Atkinson cycle in the A25A-FKS engine, it uses cEGR which also reduces pumping losses. Retarding IVC as used in Atkinson operation reduces the trapped charge in the cylinder. Adding cEGR requires that the trapped charge be increased to accommodate the fresh air and cEGR. This increase in trapped charge requires a more advanced IVC (less Atkinson) relative to the Mazda without cEGR.

**Valve Overlap:** The A25A-FKS engine has negative valve overlap everywhere except along the maximum BMEP curve (Figure 24). At low loads, hot internal EGR, typically via positive overlap with SI engines, is sometimes used to reduce pumping work and help combustion stability by increasing trapped charge temperature. At higher loads the higher temperatures have a detrimental impact on knock, which

**FIGURE 21** Effective Compression Ratio in the base OE 2014 Mazda 2.0L 13:1 geometric CR SKYACTIV-G engine, on Tier 2 fuel, 1 mm reference lift [4].



2019 US Environmental Protection Agency.

**FIGURE 22** Atkinson Ratio in the A25A-FKS engine (defined as the effective compression ratio divided by the effective expansion ratio), on Tier 2 fuel, 1 mm reference lift, (initial interval).

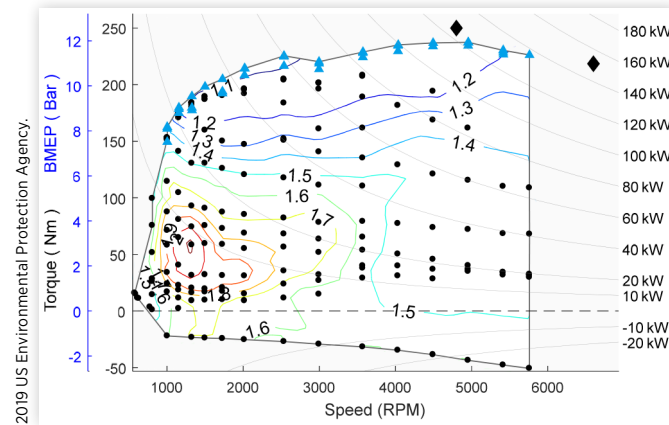


**FIGURE 23** Atkinson Ratio of the base OE Mazda 2.0L 13:1 geometric CR SKYACTIV-G engine (defined as the effective compression ratio divided by the effective expansion ratio), on Tier 2 fuel, 1 mm reference lift [4].

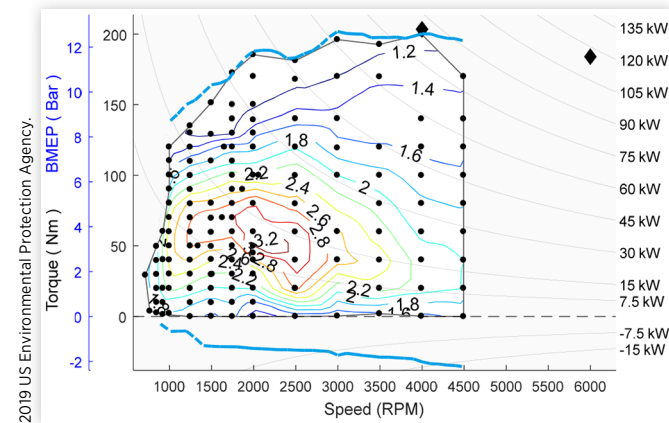
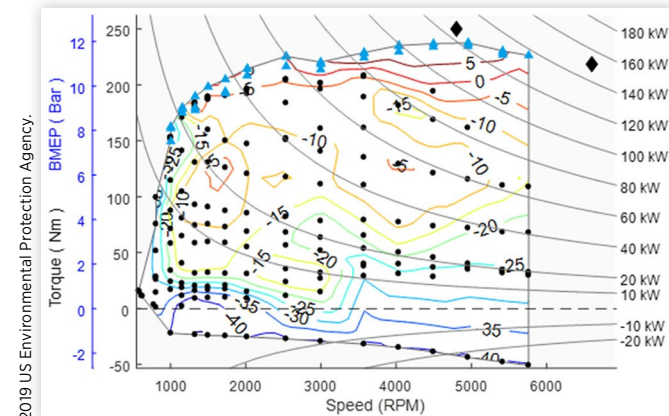


**FIGURE 24** Valve Overlap for the 2018 Toyota A25A-FKS engine, on Tier 2 fuel, 1 mm reference lift, (initial interval).



2019 US Environmental Protection Agency.

limits its use to regions where knock is not an issue. Along the torque curve a small amount of overlap is used to improve scavenging, as the intake charge flows through the cylinder and helps push out any remaining residuals.

In comparison, the valve overlap strategy employed by Mazda for their naturally aspirated Atkinson engine is quite different (Figure 25). This map has significant positive overlap in most operating areas, though in this case internal EGR is limited by the exhaust manifold tuning. The A25A-FKS has a short 4 into 1 exhaust manifold that allows pressure peaks from the exhausting cylinder to push exhaust into the cylinder that is in the gas exchange TDC (overlap). The A25A-FKS accomplishes internal EGR by maintaining a degree of negative overlap. In contrast, the Mazda incorporates a long 4-2-1 exhaust manifold to delay the arrival of the exhaust pressure peak past the overlap period, thus minimizing internal EGR. While the overlap strategies of these two engines are quite different, they both accomplished the same goal of minimizing internal EGR (residuals).

**Brake Thermal Efficiency:** Figure 26 provides two BTE maps using the steady state and high load “initial” (blue triangles) and “final” (green triangles) transient data points, as defined above in Section 2: Test Data Analysis. These data were taken using Tier 2 certification fuel, the specifications for which are given in Table 4.

For some engines, there is a significant difference between “initial” and “final” data points, both in terms of the size of the transient area of the map, and the *amount* of enrichment, fuel consumption, and emissions. Accurate characterization of the high load region is especially important when estimating fuel consumption and emissions over more highly loaded, transient vehicle drive cycles. For the Toyota A25A-FKS engine, the high load transient zone was limited to a narrow band near peak torque, and differences between initial and final values of BTE were minimal, except for small areas at low and high speeds near the peak torque line.

**BTE using Tier 3 Fuel:** The Toyota 2.5-liter A25A-FKS engine was also benchmarked using Tier 3 certification fuel (see Table 4 for the fuel specifications). After mapping the engine on Tier 2 fuel, and prior to collecting engine data on Tier 3, the engine and ECU were pre-conditioned by running through the full engine mapping process with Tier 3. This

**FIGURE 25** Valve Overlap for the base OE 2014 Mazda 2.0L 13:1 engine, on Tier 2 fuel, 1 mm reference lift [4].

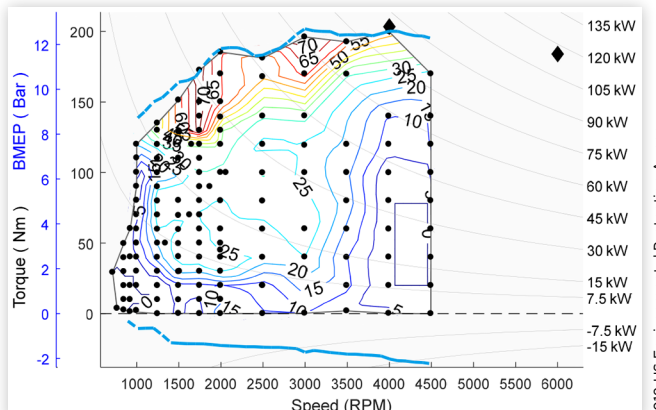
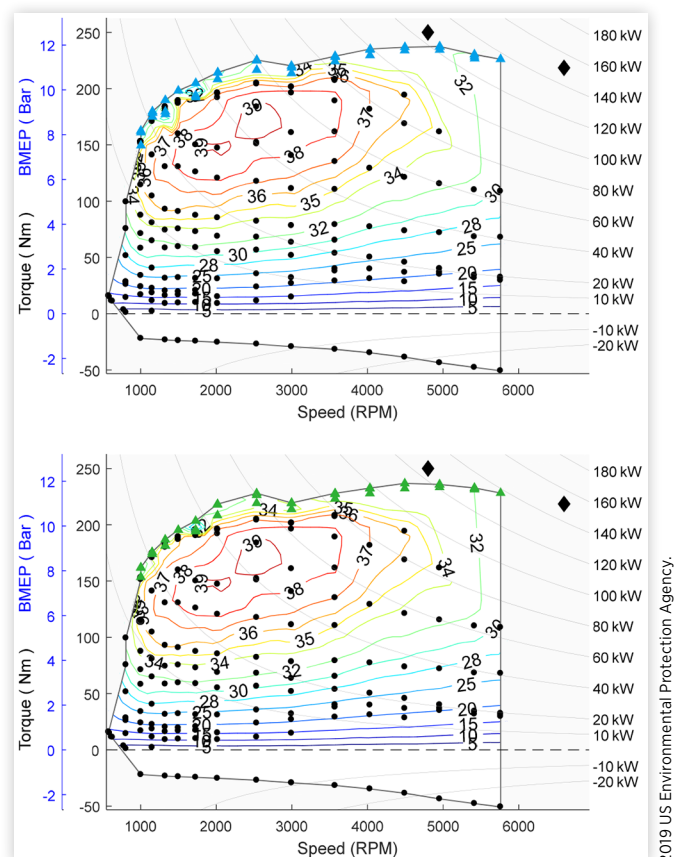


**FIGURE 26** Toyota A25A-FKS engine's BTE in the initial (top chart) and final (bottom chart) intervals, on Tier 2 fuel.

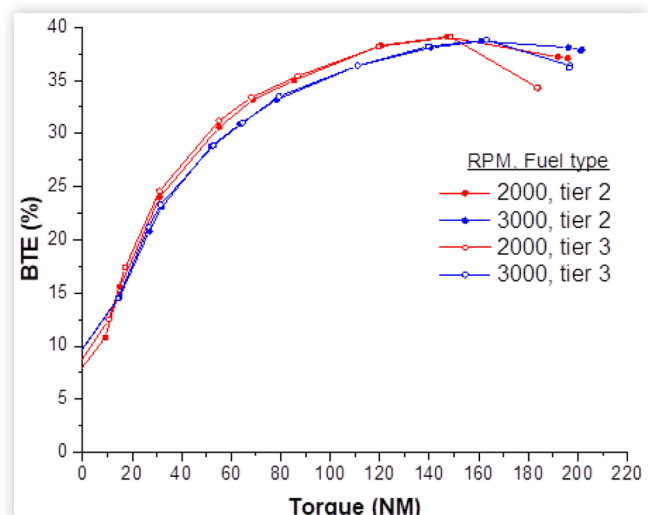


2019 US Environmental Protection Agency.

allowed the ECU to adapt to the change in octane and alcohol content across all its low to high loads for approximately three hours. Data was then collected by running through the mapping process a second time on Tier 3 fuel.

Figure 27 shows the effect of changing fuels on BTE at 2000 rpm and 3000 rpm. All data points shown in Figure 27

**FIGURE 27** Comparison of BTE running on Tier2 versus Tier 3 fuel.



2019 US Environmental Protection Agency.

are at stoichiometric air fuel (A/F) ratio; higher load points that include commanded fuel enrichment are not shown. The steady-state mapping results show very small BTE differences between the two fuels below a torque of about 160 Nm.

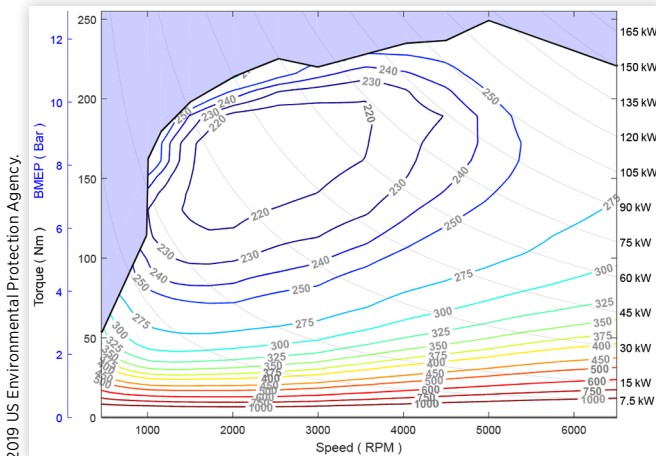
It is important to note that the minor drop in BTE observed with Tier 3 fuel does not actually correspond to an increase in CO<sub>2</sub> emissions because Tier 3 fuel has a lower carbon content than Tier 2 fuel. As described previously, using Tier 3 fuel results in a small-but-measurable overall reduction in CO<sub>2</sub> both on a fleet-wide and individual vehicle basis [23]. This is also true for the Toyota 2.5-liter A25A-FKS, as installed in the 2018 Toyota Camry.

### 3. PA's Complete Benchmarked Fuel Consumption Map of the A25A-FKS Engine

Once the benchmarking data were gathered, they were processed into a form suitable to estimate CO<sub>2</sub> emissions over the regulatory drive cycles. This work was done using techniques developed to combine the engine operating test data into a set of complete engine maps suitable for use in vehicle simulation models and other technical analyses [24].

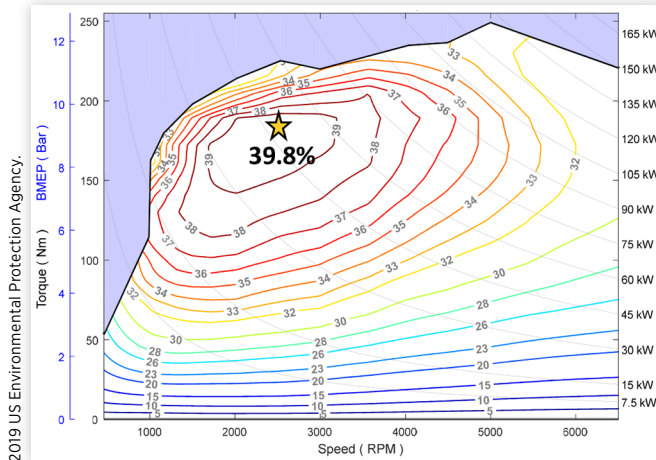
**EPA Benchmarked Maps on Tier 2 Fuel:** Figures 28 and 29 show the complete BSFC and BTE maps generated from EPA benchmarking data for the 2018 Toyota 2.5-liter A25A-FKS engine when running on Tier 2 certification fuel. The “initial” transient high load data, shown in the top chart in Figure 26, were used along with the steady-state low mid and idle low load data to generate the complete engine maps, since the two-cycle regulatory procedure [Federal Test Procedure (FTP) and Highway Fuel Economy Test (HWFET)] do not operate at the high load data points very often or long enough at any one point for the engine to transition to rich

**FIGURE 28** Complete BSFC map generated from EPA benchmarking test data of Toyota 2.5L A25A-FKS engine, on Tier 2 fuel.



2019 US Environmental Protection Agency.

**FIGURE 29** Complete BTE map generated from EPA benchmarking test data of Toyota 2.5L A25A-FKS engine, Tier 2 fuel. Peak efficiency is 39.8 percent.



operation. The measured 39.8 percent BTE is the highest measured by EPA during benchmarking of a non-hybrid 91 RON SI engine.

### Estimating Vehicle CO<sub>2</sub> Emissions Using ALPHA

To perform a quality control check of EPA’s benchmarked fuel map of the A25A-FKS engine, EPA’s ALPHA simulation model was configured to simulate the vehicle properties of a 2018 Toyota Camry used for confirmatory testing (test group JTYXV02.5P3A) listed in EPA’s 2018 Test Car List data [25]. The EPA benchmarked fuel map for the A25A-FKS engine was configured with ALPHA’s 8-speed transmission (TRX21), engine automatic start stop engine technology, a test weight of 3500 lbs., and target road load values from EPA published model year 2018 fuel economy data ( $A=21.006$  lbs.,  $B=0.17604$  lbs/mph,  $C=0.016028$  lbs/mph<sup>2</sup>) [25].

The A coefficient (lbs) represents a constant drag mostly from tire rolling resistance, B (lbs/mph) represents losses that increase with vehicle speed like bearing drag, and C (lbs/mph<sup>2</sup>) represents losses that increase with the square of vehicle speed such as aerodynamic drag. (Note that within US emission and certification procedures, vehicle characteristic values are recorded in English units rather than SI units. As the following analysis is substantially based on these characteristic values, this paper will use English units preferentially.)

Using EPA benchmarked fuel map for the A25A-FKS engine, ALPHA estimated **187.9 grams of CO<sub>2</sub> per mile** over the combined city and highway cycles used for light-duty greenhouse gas emission testing. The 2018 Toyota Camry combined city/highway test results from EPA confirmatory testing (2018 Test Car List data [25]) were **188.9 grams of CO<sub>2</sub> per mile**. The CO<sub>2</sub> emission projection from the ALPHA simulation using EPA’s benchmarked fuel map was only 0.5 percent lower than the EPA certification results for this vehicle

and are within the margin for chassis dynamometer test-to-test repeatability.

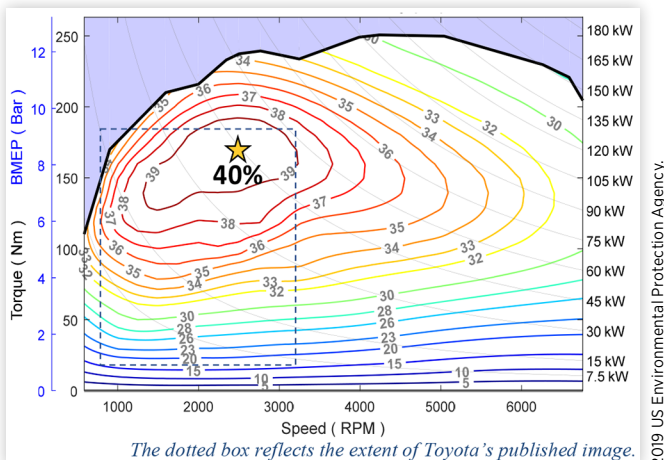
## 4. Comparing EPA's A25A-FKS BTE Map to Toyota's Published Map of Their Development Engine

In 2016 and 2017, prior to start of production of the Toyota A25A-FKS engine series, Toyota published several efficiency maps representing a developmental version of this engine [13, 14]. Figure 30 presents the complete BTE map generated by EPA, beginning with Toyota's published image [13] and using the procedures described by Dekraker [24] to produce a full map.

Of necessity, the map shown in Figure 30 includes data estimations that extend beyond the data provided in Toyota's image, which ranged from 800 rpm to 3200 rpm, and from 20 to 180 Nm (shown as the black dashed box in Figure 30).

The top chart in Figure 31 shows the difference between the BTE maps based on EPA's benchmarking data (Figure 29) and BTE map derived from the Toyota papers in Figure 30. The engine maps are generally close. The small differences seen in the heart of the map are likely due to variations between specific engines, test methods, or test instrumentation; or differences in calibration between an earlier developmental engine and the production engine in the Camry. The purple shape outlines the "heatmap" which is the approximate extent of EPA's benchmarking map of the A25A-FKS engine's operation in a 2018 vintage mid-sized vehicle over the combined city/highway regulatory cycles. There is excellent agreement of the two maps in this region, which is of primary importance for GHG/fuel economy modeling. Generally, the

**FIGURE 30** Complete BTE map generated from Toyota's publicly released map images of its 2016 2.5L developmental engine, on Tier 2 fuel.

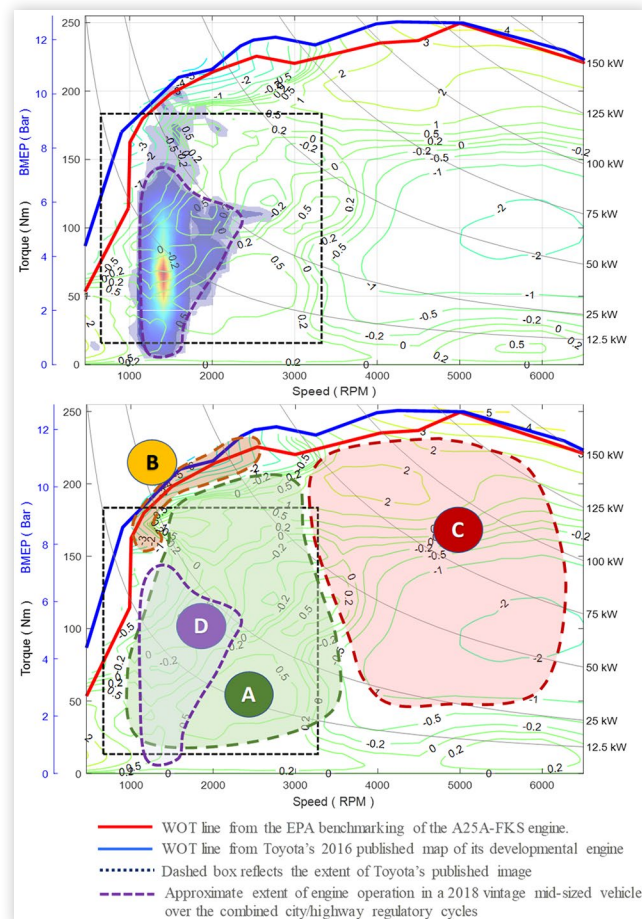


BTE maps (and the differences between them) can be classified into three key areas shown in the bottom chart of Figure 31:

**Green Zone A:** The green zone "A" in the bottom chart of Figure 31 represents a region of primary importance for U.S. GHG and Corporate Average Fuel Economy (CAFE) regulatory cycles, i.e., the combined city/highway cycles. In zone "A", the EPA and Toyota data match very well and are within +/- 0.5 percent efficiency, including Toyota's reported peak BTE of 40 percent.

**Orange Zone B:** Toyota's published maps spanned only 800 rpm to 3200 rpm, did not include data below 20 Nm, and were either clipped or uncertain above approximately 180 Nm. Thus, the high torque data in Figure 30 was estimated with a conservative roll off in efficiency up to the wide open throttle (WOT) line. The data in zone B of bottom chart of Figure 31 show that the efficiency of the EPA benchmark test data is better than the data extrapolated from Toyota's published map of their developmental engine. This is due to EPA previously over-estimating the degree of enrichment necessary in this zone, so as to create a conservative map for earlier analysis prior to benchmarking the actual production engine.

**FIGURE 31** Top chart is Efficiency (BTE) Difference Plot of A25A-FKS BTE map (Figure 29) minus the Toyota Development BTE map (Figure 30), on Tier 2 fuel. The bottom chart is the same difference plot overlaid with 3 operational zones.



**Red Zone C:** In the red zone C of the bottom chart of the Figure 31 difference map, the EPA benchmarked data was sometimes less efficient, and sometimes more efficient than the map extrapolated from Toyota's published map. The original Toyota map contained no data above 3200 rpm, making it necessary to extrapolate widely. Although it is difficult to accurately portray engine behavior in this area, the difference between the maps is under 2 percent nearly everywhere in Zone C. While even 2 percent can be significant, none of the U.S. GHG and CAFE regulatory drive cycles operate in this zone of the map. Thus, the somewhat higher degree of error in efficiency and fueling rate of the EPA estimated map based on Toyota published data was fully acceptable from a standpoint of drive-cycle modeling of efficiency, GHG, and fuel economy.

**Purple Zone D:** The purple zone D in the bottom chart of the Figure 31 difference map, outlines the heatmap for the approximate extent of EPA's benchmarking map of the A25A-FKS engine's operation in a 2018 vintage mid-sized vehicle over the combined city/highway regulatory cycles.

## Estimating Vehicle CO<sub>2</sub> Emissions Using ALPHA

As part of an analysis of different engine maps, EPA will usually run its ALPHA vehicle simulation model to study differences in CO<sub>2</sub> emissions that can occur when using data from different engines and technologies in a common exemplar vehicle [11]. This process allows the comparison of engine map data from different types and sizes of engines by using a scaling process which helps maintain comparable vehicle performance [26].

This process was used for this paper to simulate the CO<sub>2</sub> emissions that would result from using engine map data from either the 2016 Toyota developmental engine, or the 2018 production A25A-FKS engine, in the same common exemplar vehicle over the combined EPA city/highway cycles used for GHG compliance. For the purposes of this analysis, the two different engine maps (Figures 29 and 30) were treated as though they represent two completely different engines.

The three vehicle configurations used in the ALPHA simulations are shown in Table 5. The table contains the set of A, B and C road load coefficients corresponding to the road load for each of the three vehicles. The 2016 performance baseline vehicle was used to establish a baseline for the acceleration performance so that the engine maps could be properly scaled to produce comparable vehicle acceleration performance.

The analysis includes two levels of technology to help assess how sensitive the results are to the technology the engine is packaged with in the vehicle. The model year 2018 exemplar vehicle has characteristics that are roughly based on 2018 fleet-wide averages of a mid-power-to-weight ratio car [23], with the inclusion of engine automatic start stop technology. The hypothetical model year 2025 exemplar vehicle reflects an additional 7.5 percent reduction in mass, a 10 percent reduction in rolling resistance, and a 10 percent reduction in aerodynamic drag. Tier 2 fuel was specified in

all the simulations. No adjustments were made to either of the engine maps or the simulation results to adjust for any future changes due to changes in emissions aftertreatment technology.

*Results of the ALPHA simulations:* The results of the vehicle simulations in Table 6 are shown as grams of CO<sub>2</sub> per mile over the combined city and highway driving cycles. ALPHA calculated these results using the engine maps from EPA's benchmark test data of the A25A-FKS and from Toyota's published image of the map of its development version of this engine.

The orange first row in Table 6 contains a baseline estimate of 240.5 g/mile CO<sub>2</sub> from a 2016 vintage "typical" mid-sized car containing a GDI engine similar to the 2.5L Chevrolet EcoTec noted, with parameters given above in the orange column of Table 5 (2016 Performance Neutral Baseline Vehicle). This is the vehicle that was used to establish the baseline acceleration performance for the matrix of ALPHA simulation runs. ALPHA uses this information for properly resizing engine maps to maintain neutral performance for each vehicle simulation. Principles behind ALPHA's approach to engine resizing are discussed in prior work [11].

Note that each of these engines shown in the rest of the rows in Table 6 have a slightly different displacement than the 2.5L size of the A25A-FKS. This is due to the different road load requirements of the 2018 and 2025 exemplar vehicles, as well as to the differences in the WOT lines in the two engine maps affecting the calculated acceleration times. When adapting an engine to a specific vehicle's technology package and road load mix, ALPHA resizes the engine displacement so that the vehicle's acceleration performance remains within 2 percent of the baseline vehicle [10].

Table 6 shows a pair of ALPHA vehicle simulation results for a 2018 mid-sized exemplar vehicle weighing 3510 pounds; the top result uses the engine map from Toyota published image (sized to maintain performance neutrality [11]), the

**TABLE 5** Characteristics of the mid-sized vehicles used in ALPHA simulations

Vehicle Technology	2016 Performance Baseline Vehicle	2018 MY Exemplar Vehicle	2025 MY Exemplar Vehicle
Transmission	6-spd	8-spd	future 8-spd
Test Weight (lbs)	3510	3510	3270
Road Load A Coefficient (lbf)	30.620	30.620	24.833
Road Load B Coefficient (lbf/mph)	-0.0199	-0.0199	-0.0199
Road Load C Coefficient (lbf/mph <sup>2</sup> )	0.019540	0.019540	0.017586
Curb Weight Reduction (%)	0%	0%	7.5%
Aerodynamic Drag Improvement (%)	0%	0%	10%
Rolling Resistance Improvement (%)	0%	0%	10%
Engine Automatic Start Stop	no	yes	yes
Accessory	electric_EPS_HEA_REGEN	electric_EPS_HEA_REGEN	electric_EPS_HEA_REGEN

**TABLE 6** Comparison of CO<sub>2</sub> results using EPA's benchmark-based map of the A25A-FKS engine versus results using EPA's map of Toyota's published image of its developmental version of this engine.

Engine	Sized Engine Displacement	Combined FE	Combined GHG	Combined GHG % Diff
	(liters)	(mpg)	gCO <sub>2</sub> /mi	%
<b>2016 Performance Neutral Baseline Vehicle</b>				
2013 Chevrolet 2.5L Ecotec LCV	2.44 14	36.9	240.5	
<b>2018 mid-size Exemplar Vehicle</b>				
2016 Developmental Toyota 2.5L 13:1 w/cEGR (2016 Aachen paper)	2.24 14	44.6	199.1	<b>0.0%</b>
2018 Toyota 2.5L A25A-FKS 13:1 w/cEGR (EPA Benchmark)	2.26 14	44.7	198.9	<b>-0.1%</b>
<b>2025 mid-size Exemplar Vehicle</b>				
2016 Developmental Toyota 2.5L 13:1 w/cEGR (2016 Aachen paper)	1.99 14	52.8	168.2	<b>0.0%</b>
2018 Toyota 2.5L A25A-FKS 13:1 w/cEGR (EPA Benchmark)	2.00 14	52.8	168.4	<b>0.1%</b>

technologies. SAE paper 2016-01-0565 documented the results of EPA's modeling [15].

While EPA's earlier concept of adding cEGR to an existing Atkinson engine was done on a completely different engine (Mazda 2.0L 14:1 CR Skyactiv engine), it is instructive to compare the similarities and differences between EPA's concept engine and Toyota's production engine to reflect on each's effectiveness of cEGR and Atkinson Cycle in a non-HEV application.

Figure 32 shows the engine map that was generated from the GT-POWER modeling of this concept engine. This modeled map's use within EPA's midterm evaluation is documented in EPA's Proposed Determination for the Midterm Evaluation [23] and the results were validated with engine testing [16].

Figure 33 shows the differences between the EPA BTE map from the benchmarked production Toyota A25A-FKS engine (Figure 29) minus the EPA map from a scaled version of EPA's GT-POWER modeled concept of a Future Atkinson

bottom result of the 2018 pair uses the engine map from the EPA test data of the A25A-FKS engine.

Table 6 contains a second pair of ALPHA vehicle simulation results of a 2025 mid-sized exemplar vehicle weighing 3269 pounds with 10 percent lower aerodynamic resistance, 10 percent lower coefficient of rolling resistance, engine automatic start stop technology, and higher efficiency accessories [23].

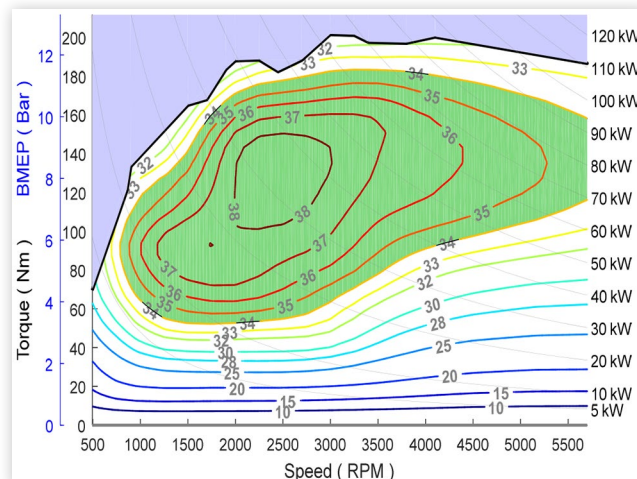
The results using the map generated from the EPA testing of Toyota's production engine have the higher CO<sub>2</sub> results of each pair over the regulatory drive cycles, corresponding to the lower BTE of the pair. The pair of simulations of the 2018 exemplar vehicle shows a 0.1 percent decrease in CO<sub>2</sub> over the regulatory cycles. The 2025 pair of simulations show a 0.1 percent increase in CO<sub>2</sub>. These results show that the two maps deliver similar CO<sub>2</sub> reduction benefits across a range of technology levels (the 2018 technology package versus the future 2025 package).

## 5. Comparing EPA's A25A-FKS BTE Map to EPA's Concept of a Future Atkinson Engine with cEGR

In 2014, as part of its analysis for the midterm evaluation of the Light-Duty GHG standards for 2022 to 2025, EPA utilized GT-POWER to model a concept for a future 2.0L Atkinson engine with increased compression ratio (14:1) and with cooled EGR (cEGR) technology. The purpose of this modeling was to learn how much CO<sub>2</sub> could be reduced from a naturally aspirated Atkinson engine through the addition of these

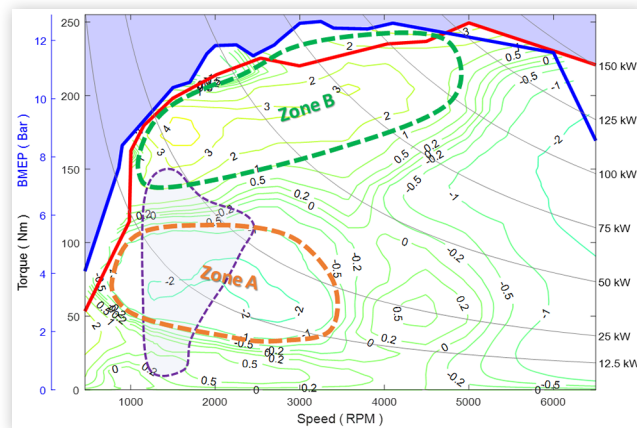
2019 US Environmental Protection Agency.

**FIGURE 32** EPA concept of a Future Atkinson 2.0L engine 14:1 geometric CR with cEGR on Tier 2 Fuel [15].



2019 US Environmental Protection Agency.

**FIGURE 33** Comparison of two BTE engine maps, Tier 2 fuel EPA BTE map from benchmarked Toyota A25A-FKS (Figure 29) minus a scaled EPA BTE map of the modeled concept of a future ATK w/cEGR (Figure 32).



2019 US Environmental Protection Agency.

with cEGR engine (Figure 32). The originally modeled map reflected an engine with a 2.0-liter displacement, but in this comparison the displacement was scaled to 2.5-liters for direct comparison to Toyota's 2.5-liter engine [11].

Outside of the zones A and B on the difference map, Figure 33 shows agreement within 0.5 percent efficiency. Within the various zones the differences are larger:

**Orange Zone A:** Within zone A, the map from the EPA test data of the A25A-FKS engine is roughly 2 percent less efficient than the map from the EPA future Atkinson with cEGR concept engine. This difference may in part be due to the concept engine model having a considerably different cEGR map versus engine speed and load, with a peak of 25 percent cEGR at 3 bar (point X in the right chart in Figure 34), which compares to the Toyota A25A-FKS test data with a peak of around 23-24 percent at 5 to 7.5 bar (point Y in Figure 34). This could cause the modeled map to have efficiency differences at 3 bar BMEP and 1000 rpm to 2500 rpm as shown in Figure 33.

It should be noted that the EPA concept engine was modeled at a higher geometric compression ratio [15], although effective compression ratio over this region varies for both the EPA concept and the Toyota engine. There are also scavenging, in-cylinder turbulence, FMEP, and other differences between the modeled EPA concept and the benchmarked Toyota A25A-FKS engine.

**Green Zone B:** Within zone B near the wide open throttle (WOT) line, the map from the EPA test data of the A25A-FKS engine is about 3 percent more efficient than the map from the EPA Atkinson/cEGR concept engine. A contributing factor could be due to the Toyota's A25A-FKS engine having less knock sensitivity than the concept engine that was modeled, due to its relative level of combustion system development. Another potential factor could be that the modeled concept could not drive cEGR flow above 2500 rpm at that load (~9 bar, Figure 34) which would lower BTE relative to the A25A-FKS which had about 10 percent cEGR at comparable operation.

**Purple Outline:** The purple dashed line in Figure 33 difference map, outlines the "heatmap" for the approximate extent of EPA's benchmarking map of the A25A-FKS engine's

operation in a 2018 vintage mid-sized vehicle over the combined city/highway regulatory cycles.

## Estimating Vehicle CO<sub>2</sub> Emissions Using ALPHA

EPA used its ALPHA model to compare the differences in CO<sub>2</sub> emissions from four engine maps over the combined EPA city/highway cycles used for GHG compliance. Simulation results for the different engine maps are shown in Table 7. A simulation run using the first, orange row in the table was used to establish a baseline for acceleration performance, so that the remaining engine maps could be properly resized to produce comparable vehicle acceleration performance.

Two sets of four simulations each were run, one set of four for a 2018 model year exemplar vehicle, and another set of four for a 2025 model year exemplar vehicle. The vehicle attributes for these exemplar vehicles are shown in Table 5. Each of the four simulations in a set used maps for the following engines:

1. 2014 Mazda 2.0L 13:1 geometric CR engine without cEGR (Figure 36) [12]
2. EPA's GT-POWER prediction for a future Atkinson engine with 14:1 geometric CR and cEGR (Figure 32) [15]
3. Toyota's development engine with 13:1 geometric CR and cEGR from Toyota data published in 2016 (Figure 30)

**TABLE 7** ALPHA simulation results for various Atkinson engine maps

Engine	Sized Engine Displacement	Combined FE	Combined GHG	Combined GHG % Diff
	(liters)	(mpg)	188.9	%

### 2016 Performance Neutral Baseline Vehicle

2013 Chevrolet 2.5L Ecotec LCV	2.44	14	36.9	240.5	
--------------------------------	------	----	------	-------	--

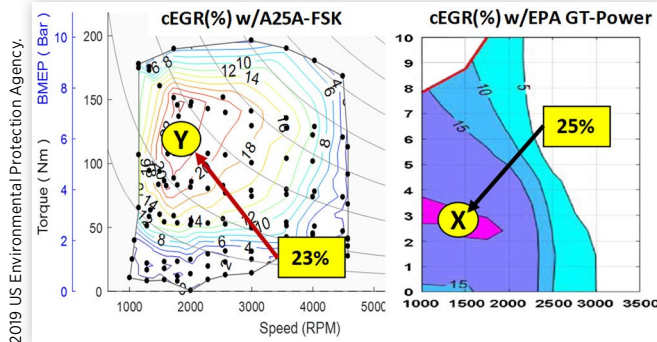
### 2018 mid-size Exemplar Vehicle

2014 Mazda SKYACTIV 2.0L 13:1	2.30	14	43.2	205.8	0.0%
Future Atkinson w/14:1 + cEGR (EPA GT-Power model)	2.30	14	44.9	198.0	-3.8%
2016 Developmental Toyota 2.5L 13:1 w/cEGR (2016 Aachen paper)	2.24	14	44.6	199.1	-3.2%
2018 Toyota 2.5L A25A-FKS 13:1 w/cEGR (EPA Benchmark)	2.26	14	44.7	198.9	-3.4%

### 2025 mid-size Exemplar Vehicle

2014 Mazda SKYACTIV 2.0L 13:1	2.09	14	50.4	176.2	0.0%
Future Atkinson w/14:1 + cEGR (EPA GT-Power model)	2.08	14	52.1	170.6	-3.2%
2016 Developmental Toyota 2.5L 13:1 w/cEGR (2016 Aachen paper)	1.99	14	52.8	168.2	-4.5%
2018 Toyota 2.5L A25A-FKS 13:1 w/cEGR (EPA Benchmark)	2.00	14	52.8	168.4	-4.4%

**FIGURE 34** Comparison of the peak percent cEGR islands of the Toyota A25A-FKS engine with Tier 2 fuel (EPA benchmark) on the left to the EPA GT-POWER model of a Future 2.0L 14:1CR with cEGR engine on the right.



4. Toyota's production 2018 A25A-FKS engine with 13:1 geometric CR and cEGR ([Figure 29](#))

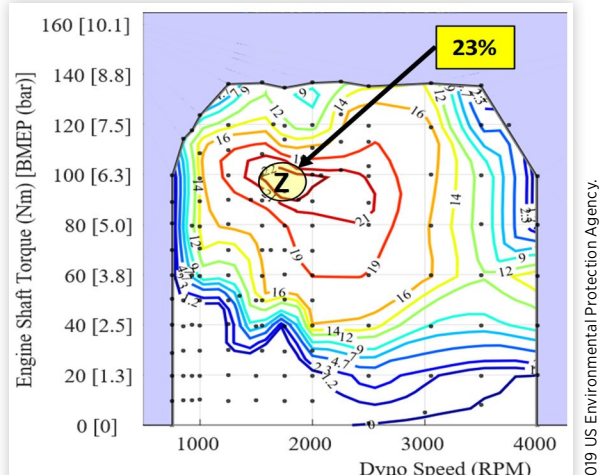
[Table 7](#) shows the percent CO<sub>2</sub> reduction that is possible, compared to the 2014 Mazda 2.0L engine which serves as the emission baseline of 205.8 grams CO<sub>2</sub> per mile for the 2018 set of simulations and 176.2 grams CO<sub>2</sub> per mile for the 2025 set of simulations. The table shows that for the 2018 model year exemplar, ALPHA predicted that the three advanced Atkinson engines were all comparable and could reduce CO<sub>2</sub> emissions by 3.2 to 3.8 percent. For the 2025 model year exemplar, ALPHA estimated that the three advanced engines could reduce CO<sub>2</sub> emissions by 3.2 to 4.5 percent.

## Test Cell Demonstration and Validation of EPA's Modeled Concept of a Future Atkinson Engine

EPA's work to demonstrate and validate its concept for a future Atkinson engine with cEGR was previously described in [\[16\]](#). The demonstration engine for this effort was built up using a EU-market version of the 2.0L Mazda SKYACTIV-G engine with a 14:1 geometric compression ratio with the addition of a developmental cEGR system and a higher energy dual-coil offset ignition system. The design of experiments and use of a higher energy ignition system resulted in some differences in the cEGR map developed for the demonstration engine relative to the EGR rates previously determined for the modeled concept engine [\[15\]](#). The cEGR calibration used during engine dynamometer testing of the demonstration engine is shown in [Figure 35](#).

Comparing the cEGR use in the Toyota A25A-FKS engine (the left chart of [Figure 34](#)) to that in the cEGR map of the

**FIGURE 35** cEGR map determined from engine testing on the EPA controlled European Mazda 14:1 engine with cEGR hardware added, Tier 2 fuel [\[16\]](#).



2019 US Environmental Protection Agency.

EPA-calibrated validation engine ([Figure 35](#)) reveals that the amount of cEGR used in the Toyota A25A-FKS engine is remarkably similar to the calibration of the EPA validation engine. In both cases the 23 percent cEGR peaks were near 2000 rpm and 6 bar, with cEGR rates tapering off near 4000 rpm and with increasing load. The EPA validation engine maintained the coefficient of variation (COV) of IMEP to less than 3 percent at all operating points.

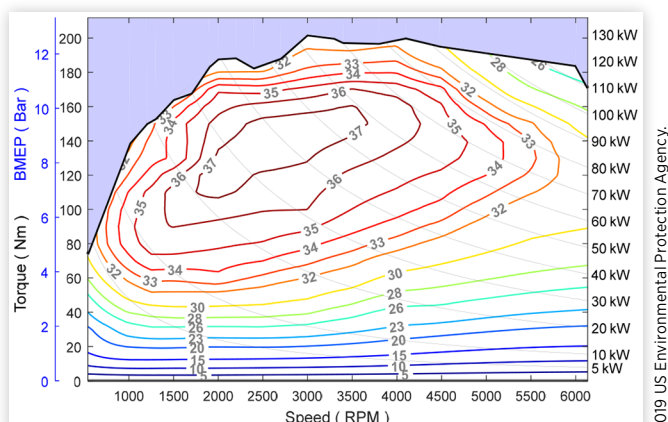
To properly compare the cEGR effects from the EPA demonstration engine (14:1 geometric CR) with the cEGR effects of the Toyota A25A-FKS engine (13:1 geometric CR), we applied the percent fuel consumption reduction effect of adding cEGR observed in the testing of the 14:1 CR demonstration engine to the base OE 2014 Mazda 2.0L 13:1 geometric CR engine map shown in [Figure 36](#). This application of the effect of cEGR onto the base Mazda 13:1 geometric CR engine map was done to remove the confounding impact of increasing geometric compression ratio in addition to adding cEGR.

The resulting transformed BTE map shown in [Figure 37](#) reveals that the effectiveness of applying cEGR at a lower (13:1) geometric compression ratio is similar to that measured for the Toyota A25A-FKS ([Figure 29](#)) except that the peak engine efficiency is shifted to a lower engine speed. The A25A-FKS peak BTE was at about 2500 rpm and 7 bar while the transformed Mazda 13:1 CR engine with cEGR applied had peak BTE at approximately 1750 rpm and 7 bar.

ALPHA simulations of the 2025 model year exemplar vehicle (defined in [Table 5](#)) with the transformed Mazda 2.0L 13:1 CR cEGR engine ([Figure 37](#)) could potentially reduce CO<sub>2</sub> emissions up to 5.7 percent over the same vehicle with the base Mazda 13:1 geometric CR engine. This cEGR effectiveness value is higher than the A25A-FKS engine's 4.4 percent, possibly because EPA's demonstration engine had its peak efficiency at lower engine speeds that were closer to where the cycles operate (see purple outline shape in [Figure 33](#), the approximate extent of engine operation in a 2018 vintage mid-sized vehicle over the combined city/highway regulatory cycles).

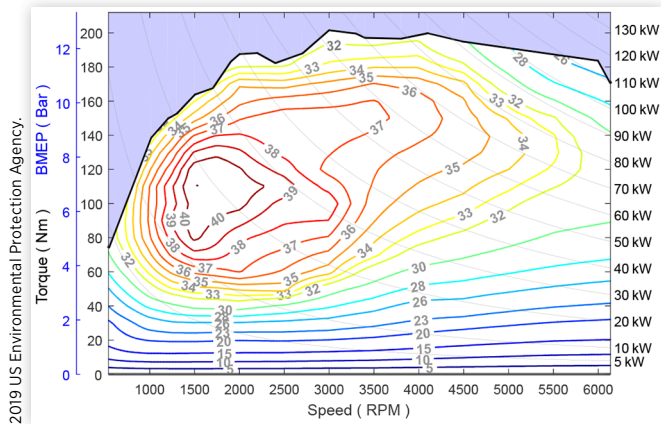
The engine dynamometer testing of this demonstration engine provided data that confirms the 3-4 percent effectiveness used for the 2017 Final Determination [\[27\]](#) was appropriate, though perhaps conservative. It should be noted that

**FIGURE 36** BTE (%) of base OE 2014 Mazda 2.0L 13:1 CR engine, on Tier 2 fuel [\[4\]](#).



2019 US Environmental Protection Agency.

**FIGURE 37** BTE (%) of a base OE Mazda 2.0L 13:1 CR engine transformed using the cEGR data from EPA demonstration engine, on Tier 2 fuel [4].



the exact Final Determination estimate depends on vehicle type and tech package and includes both increasing the geometric CR from 13:1 to 14:1 and the addition of cEGR.

## 6. Potential for Improving Efficiency Using Cylinder Deactivation

The fuel efficiency map shown in Figure 29 of Section 3 shows that the A25A-FKS engine achieves excellent efficiency with a peak BTE of approximately 40 percent and a broad range that exceeds 35 percent. Yet even for such an efficient engine, use of cylinder deactivation may offer additional improvement by expanding the high efficiency region of the Toyota A25A-FKS engine. This section explores the effect of the addition of both fixed discrete and full continuous cylinder deactivation, which are both currently available technologies that could further improve the fuel efficiency of the A25A-FKS engine.

Full continuous cylinder deactivation (deacFC) enables any number of cylinders to be deactivated, while partial discrete cylinder deactivation (deacPD) enables only certain cylinders to be deactivated. Both systems reduce pumping work and cylinder heat loss at low and medium engine loads but deacFC is more effective because of its greater flexibility.

DeacFC was pioneered by Tula Technology and Delphi [28 - 30] and entered series production on model year 2019 GM Silverado 5.3L and 6.2L engines [31]. DeacPD has been adopted by numerous manufacturers for years, reaching 10.4 percent of the model year 2016 U.S. market production volume with 1,692,733 engines built by FCA, GM, Honda, Mercedes-Benz and VW according to EPA OTAQ compliance data and Ward's Automotive Yearbook [32]. DeacPD has also been applied to the model year 2018 2.5L Mazda SKYACTIV-G Atkinson Cycle engine that serves as the base engine for the Mazda CX-5 and Mazda6.

Engine technology analysis and full vehicle simulations were used to estimate the additional effectiveness that deacFC and deacPD could bring to the Toyota A25A-FKS engine. For this paper, the percent effectiveness of deacFC or deacPD is the percent reduction in fuel consumption relative to same engine without cylinder deactivation. For this assessment the effectiveness is assumed to be primarily a function engine load and does not vary with engine speed over the range of speeds in which deacFC or deacPD is used.

The effectiveness of adding cylinder deactivation to the Toyota A25A-FKS engine was assessed using two methods to provide a range of improvement rather than a single estimate:

1. Method 1 uses prior data from EPA benchmarking of deacFC and deacPD technology on other engines and adjusts the effectiveness to account for differences between engines including cylinder count, cEGR, and whether deacFC or deacPD is used.
2. Method 2 uses deacFC effectiveness data provided by Tula Technology (whose technology is being licensed in the model year 2019 GM Silverado) and adjusts the effectiveness to account for cylinder count, cEGR and whether deacFC or deacPD is used.

## Method 1: Estimating the Effectiveness of Cylinder Deactivation Using Data from Prior EPA Benchmarking

In this method, the effectiveness of adding deacFC or deacPD to the Toyota A25A-FKS was estimated using data from four sources:

1. EPA benchmarking of a 2011 GMC Yukon 6.2L L94 V8 equipped with deacFC [8]
2. preliminary EPA benchmarking of a 2015 VW Jetta 1.8L turbo EA888 I4 equipped with deacFC
3. publications by Tula Technology [30, 33]
4. additional engineering analysis

A comparison of the GM L94, VW EA888 and Toyota A25A-FKS engines is shown in Table 8.

**Determining deacFC effectiveness:** The effectiveness of deacFC on the eight-cylinder L94 was previously measured by EPA [8] and is represented by the top curve (green) in Figure 38. The effectiveness from that study was adjusted downward to account for the lower cylinder count of the Toyota A25A-FKS I4 engine. The amount of adjustment is the ratio of the published effectiveness of deacFC on the four-cylinder EA888 [30] and the published effectiveness of deacFC on the eight-cylinder L94 [30]. This reduced effectiveness is represented by the middle curve (red) in Figure 38.

The deacFC effectiveness curve was then further reduced to account for the amount of cEGR on the A25A-FKS engine

**TABLE 8** Engine specifications

	<b>GM L94</b>	<b>VW EA888</b>	<b>Toyota A25A-FKS</b>
Design	Naturally aspirated 6.2L V8	Turbocharged 1.8L I4	Naturally aspirated 2.5L I4
Camshaft phasing	Camshaft in block phasing	Intake phasing	Intake and exhaust phasing
EGR	No	No	cEGR
CR	10.4	9.6	13.0

2019 US Environmental Protection Agency.

shown as the black effectiveness curve in [Figure 38](#). Both cEGR and cylinder deactivation reduce pumping losses and care must be taken not to double count this benefit. This method was applied to the deacFC for the A25A-FKS engine, using cEGR rates as shown in [Figure 18](#).

To determine the amount by which the deacFC effectiveness curve should be reduced to account for cEGR, it is assumed the volume flow of cEGR+air at a particular engine load on a cEGR engine allows a cylinder deactivation benefit equal to the cylinder deactivation benefit on a non-cEGR engine at a higher load, where the volume flow of air equals the volume flow of cEGR+air on the cEGR engine. Mass flow, temperature and composition of cEGR and air, measured on the A25A-FKS, were used to determine how much additional volume flow cEGR adds at the point of mixing, from which the reduction in cylinder deactivation effectiveness could be calculated.

As an example, consider the deacFC effectiveness curve for an I4 without cEGR (red curve in [Figure 38](#)). At 2 bar BMEP, deacFC offers a 9 percent benefit and at 2.3 bar BMEP deacFC offers a smaller benefit - 8 percent. If cEGR is added to the engine and the total volume of cEGR+air at 2 bar equals the volume of air that the engine uses at 2.3 bar BMEP without cEGR, then the effectiveness of deacFC at 2 bar with cEGR becomes the effectiveness of deacFC at 2.3 bar without cEGR (8 percent).

There are other benefits that are enabled by deacFC from other features such as the engine's deceleration fuel cut-off (DFCO), operation during zero pedal gliding, and interaction

with Atkinson Cycle, interaction with cEGR and knocking at high load.

For example, deacFC can be used to deactivate all engine valves during deceleration fuel cut-off (DFCO) events, which avoids filling the three-way catalyst with oxygen. Then upon exiting DFCO, extra fuel doesn't have to be injected (rich engine operation) to consume the oxygen stored on the catalyst during the DFCO. This is an additional efficiency benefit of deacFC relative to deacPD and engines without cylinder deactivation.

EPA's full vehicle simulation (ALPHA) estimates that by avoiding the extra fuel injection after DFCO events deacFC can reduce CO<sub>2</sub> by an extra 0.1 percent on a model year 2025 mid-size exemplar passenger car with a downsized A25A-FKS engine (described in the next sub-section) using the black effectiveness curve shown in [Figure 38](#) over the combined drive cycle (FTP75+HWFET).

DeacFC also allows fuel to be saved during a DFCO event because deactivating valves reduces pumping losses and allows the vehicle to glide more easily. This reduction in pumping losses during DFCO events is estimated to save 0-1.5 percent CO<sub>2</sub> depending on drive cycle and vehicle calibration. The interaction between deacFC and gliding benefit is not currently modeled but is the subject of ongoing work.

Both the EA888 and A25A-FKS engines use intake valve phasing to implement Miller or Atkinson cycle at part load, respectively, so it is assumed that the interaction between deacFC and Atkinson cycle is approximately accounted for within this analysis.

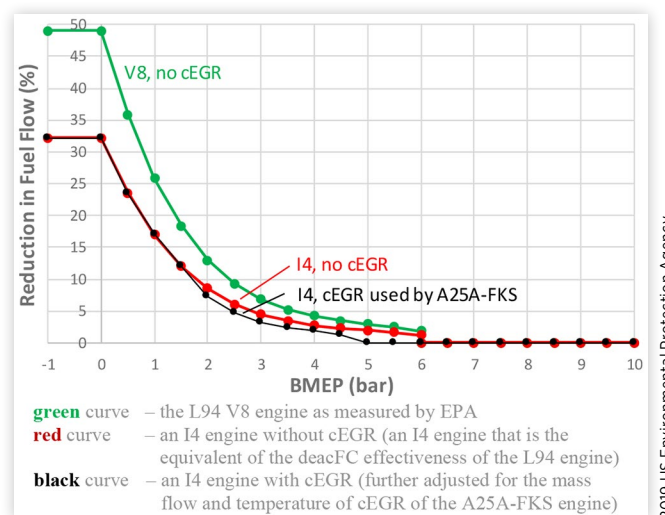
Cooled EGR can reduce knocking tendency at high load, which can potentially increase the effectiveness of cEGR because firing cylinders operating near full load and using cEGR may require less enrichment or spark retard. However, the extent to which cEGR is used under full load on a naturally aspirated engine is typically limited for peak torque considerations, so this synergistic behavior is ignored in this analysis.

The engine conditions under which deacFC is allowed to operate (i.e., its fly zone) were estimated based on EPA benchmarking of the GM L94 and VW EA888 engines with deacFC [8]:

- T<sub>coolant</sub>>44°C (reached after the first 67 seconds of operation for the 2015 VW Jetta EA888 operating over the FTP75)
- Engine speed = 940-2500 rpm [7, 8]
- Transmission Gear = 2 to 6 [8]

**Determining deacPD effectiveness:** To estimate the effectiveness of deacPD on an A25A-FKS engine, the deacFC effectiveness curve described above was modified to allow only two states of operations: firing 2 cylinders or firing 4 cylinders. This results in an effectiveness curve that only has two levels: no reduction in fuel flow while firing on four cylinders, and a fixed reduction in fuel flow while firing on two cylinders. The fly zone of deacPD is assumed to be the same as for deacFC.

**Estimating vehicle CO<sub>2</sub> emissions using ALPHA:** EPA's full vehicle simulation model was used to compare the differences in CO<sub>2</sub> emissions for the A25A-FKS engine with and without deacPD and deacFC. The ALPHA drive cycle simulation accounts for several transient fueling penalties. These

**FIGURE 38** EPA estimate of deacFC effectiveness (percent reduction of BSFC).

include spark retard for torque management during gear shifts, fueling penalty proportional to the rate of change of engine torque, extra fuel added upon exiting DFCO (if the engine uses deacPD or no cylinder deactivation), and engine startup and warmup effects. Details on these transient effects have been previously published [11, 26].

Table 9 shows the estimated benefit of adding deacFC or deacPD to the A25A-FKS engine, downsized to 2.0L and used in a model year 2025 mid-size exemplar passenger car (medium power to weight, low road load defined in Table 5) over the combined drive cycle (FTP75+HWFET), using prior EPA benchmarking and the effectiveness adjustments described above. The addition of deacFC is estimated to achieve a 3.3 percent reduction in CO<sub>2</sub> over the already efficient A25A-FKS engine, while the simpler deacPD is estimated to achieve a 1.4 percent reduction in CO<sub>2</sub>.

For reference, EPA previously estimated a 2.6 percent combined cycle reduction in CO<sub>2</sub> for adding deacFC to a Honda L15B7 engine downsized to 1.42-liter in a 2025 mid-size exemplar passenger car [1]. This CO<sub>2</sub> reduction is less than the 3.3 percent shown in Table 9, which is reasonable because the result in Table 9 is for a larger, un-boosted engine, which spends more time at low load where deacFC provides a larger benefit.

The CO<sub>2</sub> effectiveness benefit estimated for the application of deacPD to the Toyota A25A-FKS engine is also comparable to the approximately 2 percent difference in CO<sub>2</sub> between front-wheel drive versions of the model year 2017 and 2018 Mazda CX-5, the latter having deacPD but otherwise both of which are identical with respect to road loads, ETW, transmission, final drive, etc. [25].

## Method 2: Estimate the Effectiveness of Cylinder Deactivation Using Data from a deacFC Supplier

In this section, rather than adjusting a deacFC effectiveness curve from EPA benchmarking of a V8 demonstration engine to an I4 engine, effectiveness data provided by Tula Technology from a 4-cylinder VW EA888 demonstration engine is used instead. Tula requested that the effectiveness data remain confidential but has allowed use of their data in the ALPHA vehicle simulation.

The same general methodology was followed as described in the previous section (Method 1): The deacFC effectiveness curve from the EA888 was modified to account for cEGR and the drive cycle simulations accounted for transient effects. Improved vehicle gliding during DFCO with deacFC, and potential reduction in knocking tendency when cEGR is used with deacFC or deacPD were not modeled. The effectiveness of deacPD was estimated by modifying the deacFC curve to allow only two states of operation: firing 2 cylinders or firing 4 cylinders.

**Estimating vehicle CO<sub>2</sub> emissions using ALPHA:** Table 10 shows the estimated benefit of adding deacFC or deacPD to

**TABLE 9** Effect of deacFC and deacPD on vehicle fuel economy and CO<sub>2</sub> (2025 exemplar vehicle) using data from prior EPA benchmarking of supplier demonstration vehicles with cylinder deactivation.

Engine	Type of cylinder Deac	Sized Engine Displacement		Combined FE	Combined GHG	Delta from Mazda	Effect of Adding Cylinder Deac.
		(liters)	(mpg)				
2014 Mazda SKYACTIV 2.0L 13:1	none	2.09	14	50.4	176.2	0.0%	
2018 Toyota 2.5L A25A-FKS 13:1 w/cEGR (EPA Benchmark)	none	2.00	14	52.8	168.4	-4.4%	0.0%
	deacPD	2.00	14	53.5	166.0	-5.8%	-1.4%
	deacFC	2.00	14	54.6	162.8	-7.6%	-3.3%
Future EGRB-24 + cEGR (EPA model)	none	1.22	14	54.6	162.7	-7.7%	

2019 US Environmental Protection Agency.

**TABLE 10** Effect of deacFC and deacPD on vehicle fuel economy and CO<sub>2</sub> (2025 exemplar vehicle) using data from cylinder deactivation supplier.

Engine	Type of cylinder Deac	Sized Engine Displacement		Combined FE	Combined GHG	Delta from Mazda	Effect of Adding Cylinder Deac.
		(liters)	(mpg)				
2014 Mazda SKYACTIV 2.0L 13:1	none	2.09	14	50.4	176.2	0.0%	
2018 Toyota 2.5L A25A-FKS 13:1 w/cEGR (EPA Benchmark)	none	2.00	14	52.8	168.4	-4.4%	0.0%
	deacPD	2.00	14	54.0	164.6	-6.6%	-2.3%
	deacFC	2.11	14	57.3	155.1	-11.9%	-7.9%
Future EGRB-24 + cEGR (EPA model)	none	1.22	14	54.6	162.7	-7.7%	

2019 US Environmental Protection Agency.

the A25A-FKS engine, downsized to 2.01L and used in a 2025 mid-size exemplar passenger car (medium power to weight, low road load defined in Table 5) over the combined drive cycle (FTP75+HWFET), using supplier deac effectiveness data and accounting for cEGR. The addition of deacFC is estimated to achieve a 7.9 percent reduction in CO<sub>2</sub> over the already highly efficient A25A-FKS engine, while the simpler deacPD is estimated to achieve a 2.3 percent reduction in CO<sub>2</sub>.

EPA plans to continue to evaluate the effectiveness of both deacPD and deacFC as original equipment manufacturers and suppliers introduce the technology on new production and demonstration vehicles. EPA has active benchmarking programs to assess deacPD in a 2018 Mazda 6 with a naturally aspirated 2.5L engine with deacPD, a 2019 Chevrolet Silverado with naturally aspirated 5.3L engine with deacFC, and a Tula deacFC demonstration vehicle utilizing a 2015 VW Jetta 1.8L turbo Miller cycle engine.

## Summary/Conclusions

EPA's benchmarking test method of mapping an engine by tethering a vehicle to an engine in an engine dynamometer cell has been expanded to include measurement of valve timing (especially important for Atkinson and Miller Cycle

engines), and measurement of cEGR flow, which allowed EPA to evaluate the effectiveness of these important new GHG-reducing technologies against previous estimates.

The BTE map for the Toyota A25A-FKS engine developed from EPA benchmark testing demonstrated the highest efficiency of any publicly available map for a production non-hybrid spark-ignition internal combustion engine and yet is still designed to run on 91 RON fuel. The map developed from benchmarking data is nearly identical to a map previously published by Toyota for their developmental version of this same 2.5-liter engine.

EPA's analysis of the Toyota A25A-FKS benchmarking data shows an effectiveness of cEGR technology in reducing CO<sub>2</sub> emissions over the combined FTP and HWFET cycles of approximately 4 percent compared to an Atkinson engine without cEGR. The Toyota A25A-FKS application, both in terms of amount of cEGR and CO<sub>2</sub> emission reduction, is in good agreement with data from earlier phases of EPA's demonstration program for its concept for a Future Atkinson engine with cEGR.

Potential incremental efficiency improvements remain for the technology package found in the Toyota A25A-FKS engine through the application of cylinder deactivation technology already implemented in current production engines, including both fixed discrete (deacPD) and full continuous (deacFC) versions of cylinder deactivation. Application of deacPD was estimated to provide a 1.4 percent to 2.3 percent CO<sub>2</sub> reduction from the production Toyota A25A-FKS, while deacFC was estimated to provide a 3.7 percent to 7.9 percent CO<sub>2</sub> reduction compared to base Toyota A25A-FKS engine, even while neglecting the vehicle gliding benefit of deacFC.

When applied to a standard midsized car, the Toyota A25A-FKS engine with deacFC comes close to meeting or possibly improving upon EPA's 2010 estimate for CO<sub>2</sub> emissions from the future 24-bar cEGR turbocharged engine (EGRB24) [34], which was previously the most effective engine technology considered by EPA.

This and other studies have shown that naturally aspirated engines have adopted most of the technologies reviewed in EPA's light-duty vehicle midterm evaluation [23, 27] and that the technology effectiveness achieved by new production engines are similar to the values projected in the rulemaking. The Toyota A25A-FKS makes use of Atkinson Cycle, a high authority and fast intake camshaft phaser, a hydraulic exhaust camshaft phaser, long stroke/bore ratio (to promote good tumble and reduce heat loss and friction), a fuel injection system with port and direct injection, high geometric compression ratio and high expansion ratio, cEGR, and various friction reduction technologies including an offset crankshaft and a low-friction piston skirt design.

Additional benefits are possible through application of deacFC, as well as incremental improvements in existing technologies, and over the longer term, through additional engine design changes.

Boosted engines can also be improved further, by valve timing improvements, Miller cycle, deacFC, the increased degrees of freedom offered via variable compression ratio engines such as Nissan's VC-T [35] and unconventional step-change technologies like spark-controlled compression ignition (SPCCI) anticipated in Mazda's upcoming SKYACTIV-X engine [36].

## References

1. Stuhldreher, M., Kargul, J., Barba, D., McDonald, J. et al., "Benchmarking a 2016 Honda Civic 1.5-liter L15B7 Turbocharged Engine and Evaluating the Future Efficiency Potential of Turbocharged Engines," SAE Technical Paper [2018-01-0319](#), 2018, doi:[10.4271/2018-01-0319](#).
2. Stuhldreher, M., Schenk, C., Brakora, J., Hawkins, D. et al., "Downsized Boosted Engine Benchmarking and Results," SAE Technical Paper [2015-01-1266](#), 2015, doi:[10.4271/2015-01-1266](#).
3. U.S. EPA, "2013 Chevrolet Malibu 2.5 L Engine Mapping Test Package," Docket number EPA-HQ-OAR-2015-0827-0532, <https://www.epa.gov/sites/production/files/2016-10/2013-chevrolet-malibu-2.5l-engine-mapping-test-package-06-20-16.zip>, last accessed on Jan. 3, 2018.
4. U.S. EPA, "2014 Mazda 2.0 L Skyactiv 13-1 Tier 2 Fuel - Engine Mapping Core Test Package," Docket number EPA-HQ-OAR-2015-0827-0533, <https://www.epa.gov/sites/production/files/2016-10/2014-mazda-2.0l-skyactiv-13-1-tier2-fuel-engine-mapping-core-test-package-06-28-16.zip>, last accessed Jan. 3, 2018.
5. U.S. EPA, "2015 Ford F150 2.7 L Tier 2 Fuel - Engine Mapping Core Test Package," Docket number EPA-HQ-OAR-2015-0827-0534, <https://www.epa.gov/sites/production/files/2016-10/2015-ford-f150-2.7l-tier2-fuel-engine-mapping-core-test-package-06-21-16.zip>, last accessed Jan. 3, 2018.
6. Ellies, B., Schenk, C., and Dekraker, P., "Benchmarking and Hardware-in-the-Loop Operation of a 2014 MAZDA SkyActiv 2.0 L 13:1 Compression Ratio Engine," SAE Technical Paper [2016-01-1007](#), 2016, doi:[10.4271/2016-01-1007](#).
7. Stuhldreher, M., "Fuel Efficiency Mapping of a 2014 6-Cylinder GM EcoTec 4.3 L Engine with Cylinder Deactivation," SAE Technical Paper [2016-01-0662](#), 2016, doi:[10.4271/2016-01-0662](#).
8. Bohac, S., "Benchmarking and Characterization of Two Cylinder Deactivation Systems - Full Continuous and Partial Discrete," SAE Oral-Only Presentation, SAE World Congress, 2018.
9. Lee, B., Lee, S., Cherry, J., Neam, A. et al., "Development of Advanced Light-Duty Powertrain and Hybrid Analysis Tool," SAE Technical Paper [2013-01-0808](#), 2013, doi:[10.4271/2013-01-0808](#).
10. Kargul, J., Moskalik, A., Barba, D., Newman, K. et al., "Estimating GHG Reduction from Combinations of Current Best-Available and Future Powertrain and Vehicle Technologies for a Midsized Car Using EPA's ALPHA Model," SAE Technical Paper [2016-01-0910](#), 2016, doi:[10.4271/2016-01-0910](#).
11. Dekraker, P., Kargul, J., Moskalik, A., Newman, K. et al., "Fleet-Level Modeling of Real World Factors Influencing Greenhouse Gas Emission Simulation in ALPHA," SAE Int. J. Fuels Lubr. 10(1):2017, doi:[10.4271/2017-01-0899](#).
12. US Environmental Protection Agency, "Benchmarking Advanced Low Emission Light-Duty Vehicle Technology," <https://www.epa.gov/vehicle-and-fuel-emissions-testing/>

- [benchmarking-advanced-low-emission-light-duty-vehicle-technology](#), accessed Nov. 6, 2018.
13. Murase, E. and Shimizu, R., "Innovative Gasoline Combustion Concepts for Toyota New Global Architecture," in *25th Aachen Colloquium - Automobile and Engine Technology*, 2016.
  14. Toda, T., Sakai, M., Hakariya, M., and Kato, T., "The New Inline 4 Cylinder Gasoline Engine with Toyota New Global Architecture Concept," in *38th International Vienna Motor Symposium*, 2017.
  15. Lee, S., Schenk, C., and McDonald, J., "Air Flow Optimization and Calibration in High-Compression-Ratio Naturally Aspirated SI Engines with Cooled-EGR," SAE Technical Paper [2016-01-0565](#), 2016, doi:[10.4271/2016-01-0565](#).
  16. Schenk, C. and Dekraker, P., "Potential Fuel Economy Improvements from the Implementation of cEGR and CDA on an Atkinson Cycle Engine," SAE Technical Paper [2017-01-1016](#), 2017, doi:[10.4271/2017-01-1016](#).
  17. U.S. Code of Federal Regulations, Title 40, Part 1065, §1065.130, Jan. 1, 2018.
  18. U.S. EPA, "Light-Duty Automotive Technology, Carbon Dioxide Emissions, and Fuel Economy Trends: 1975 through 2017," Report No. EPA-420-R-18-001, Jan. 2018.
  19. Hakariya, M., Toda, T., and Sakai, M., "The New Toyota Inline 4-Cylinder 2.5L Gasoline Engine," SAE Technical Paper [2017-01-1021](#), 2017, doi:[10.4271/2017-01-1021](#).
  20. Stuhldreher, M., Kim, Y., Kargul, J., Moskalik, A. et al., "Testing and Benchmarking a 2014 GM Silverado 6L80 Six Speed Automatic Transmission," SAE Technical Paper [2017-01-5020](#), 2017, doi:[10.4271/2017-01-5020](#).
  21. "Toyota Handbook," TIN517B Fall 2017 New Technology Update.
  22. Yamaji, K., Tomimatsu, M., Takagi, I., Higuchi, A. et al., "New 2.0L 14 Gasoline Direct Injection Engine with Toyota New Global Architecture Concept," SAE Technical Paper [2018-01-0370](#), 2018, doi:[10.4271/2018-01-0370](#).
  23. U.S. EPA, "Proposed Determination on the Appropriateness of the Model Year 2022-2025 Light-Duty Vehicle Greenhouse Gas Emissions Standards under the Midterm Evaluation Technical Support Document," §2.3.4.1.9.1 -Effectiveness Data Used and Basis for Assumptions, Document Number EPA-420-R-16-021, Nov. 2016.
  24. Dekraker, P., "Constructing Engine Maps for Full Vehicle Simulation Modeling," SAE Technical Paper [2018-01-1412](#), 2018, doi:[10.4271/2018-01-1412](#).
  25. US Environmental Protection Agency, "Data on Cars Used for Testing Fuel Economy," <https://www.epa.gov/compliance-and-fuel-economy-data/data-cars-used-testing-fuel-economy>, accessed Nov. 28, 2018.
  26. Dekraker, P., Stuhldreher, M., and Kim, Y., "Characterization Factors Influencing SI Engine Transient Fuel Consumption for Vehicle Simulation in ALPHA," SAE Technical Paper [2017-01-0533](#), 2017, doi:[10.4271/2017-01-0533](#).
  27. "U.S. EPA Final Determination on the Appropriateness of the Model Year 2022-2025 Light-Duty Vehicle Greenhouse Gas Emissions Standards under the Midterm Evaluation," Document Number EPA-420-R-17-002, Jan. 2017.
  28. Serrano, J., Routledge, G., Lo, N., Shost, M. et al., "Methods of Evaluating and Mitigating NVH when Operating an Engine in Dynamic Skip Fire," SAE Technical Paper [2014-01-1675](#), 2014, doi:[10.4271/2014-01-1675](#).
  29. Eisazadeh-Far, K. and Younkins, M., "Fuel Economy Gains Through Dynamic-Skip-Fire in Spark Ignition Engines," SAE Technical Paper [2016-01-0672](#), 2016, doi:[10.4271/2016-01-0672](#).
  30. Younkins, M., Tripathi, A., Serrano, J., Fuerst, J. et al., "Dynamic Skip Fire: The Ultimate Cylinder Deactivation Strategy," in *38th International Vienna Motor Symposium*, 2017.
  31. Younkins, M., Ortiz-Soto, E., Wilcutts, M., Fuerst, J. et al., "Dynamic Skip Fire: New Technologies for Innovative Propulsion Systems," in *39th International Vienna Motor Symposium*, 2018.
  32. *Ward's Automotive Yearbook 2017* (). ISBN:978-0-910589.
  33. Fuschetto, J., Eisazadeh-Far, K., Younkins, M., Carlson, S. et al., "Dynamic Skip Fire in Four-Cylinder Spark Ignition Engines: Fuel Economy Gains and Pollutant Emissions Reductions," SAE Oral-Only Presentation, SAE World Congress, 2017.
  34. Ricardo, "Computer Simulation of Light-Duty Vehicle Technologies for Greenhouse Gas Emission Reduction in the 2020-2025 Timeframe," EPA-420-R-11-020, 2011.
  35. Kosowatz, J., "Rekindling the Spark," *Mechanical Engineering Magazine* 139(11):28-33, Nov. 2017.
  36. MAZDA Next-Generation Technology - PRESS INFORMATION, Oct. 2017, [https://ljjylmozio83m2nkr2v293mp-wpengine.netdna-ssl.com/wp-content/uploads/2017/10/02\\_ENG\\_Mazda\\_Next\\_Generation\\_Technology\\_Press\\_Information.pdf](https://ljjylmozio83m2nkr2v293mp-wpengine.netdna-ssl.com/wp-content/uploads/2017/10/02_ENG_Mazda_Next_Generation_Technology_Press_Information.pdf).
  37. Toyota, "Toyota Unveils Completely Redesigned Camry - Responsive Driving Performance and Stunning Looks Built on All-New Toyota New Global Architecture (TNGA) Platform and Powertrain," Toyota Press Release, 2017, <https://newsroom.toyota.co.jp/en/detail/17680157>.
  38. Toyota, "All-New 2019 Toyota RAV4 Breaks the Mold for the Segment It Created," Toyota Press Release, 2018, <https://pressroom.toyota.com/releases/all-new+2019+toyota+rav4+brea>ks+the+mold+for+the+segment+it+created.htm.
  39. Toyota, "Attainable Premium, Actualized: All-New 2019 Toyota Avalon Beams Effortless Sophistication, Style, and Exhilaration at the 2018 North American International Auto Show," Toyota Press Release, 2018, <https://toyotanews.pressroom.toyota.com/releases/attainable+premium+actualized+all+new+2019+toyota+avalon+beams+effortless+sophistication+style.htm>.
  40. Toyota, "Hatch Is Back! All-New 2019 Toyota Corolla Hatchback Wows with Loads of Style, Dynamic Performance, and Technology," Toyota Press Release, 2018, <https://toyotanews.pressroom.toyota.com/releases/hatch+is+back+all-new+2019+toyota+corolla+hatchback+wo>ws+loads+style+dynamic+technology.htm.

## Contact Information

### Mark Stuhldreher

National Center for Advanced Technology  
 US EPA - National Vehicle and Fuel Emissions Laboratory  
 734-214-4922  
[Stuhldreher.mark@epa.gov](mailto:Stuhldreher.mark@epa.gov)

## Acknowledgments

The authors would like to thank Andrew Moskalik, Kevin Newman, Karla Butters, Brian Olson, Raymond Kondel, Mathew Coon, Mike Murphy, and Greg Davis in the National Center of Advanced Technology at the National Vehicle and Fuel Emissions Laboratory for their assistance and contribution to perform necessary engine testing and ALPHA modeling.

## Disclaimer

This is a declared work of the U.S. Government and is not subject to U.S. copyright protection. Foreign copyrights may apply. The U.S. Government assumes no liability or responsibility for the contents of this paper or the use of this paper, nor is it endorsing any manufacturers, products, or services cited herein and any trade name that may appear in the paper has been included only because it is essential to the contents of the paper.

## Definitions/Abbreviations

**ACFM** - Actual Cubic Feet per Minute

**A/F** - Air Fuel ratio

**AKI** - Anti-Knock Index

**ALPHA** - Advanced Light-duty Powertrain and Hybrid Analysis Tool

**BMEP** - Brake Mean Effective Pressure

**BSFC** - Brake Specific Fuel Consumption

**BTE** - Brake Thermal Efficiency

**b** - Regression Offset

**CAD** - Crank Angle Domain *or* Crank Angle Degrees

**CAFE** - Corporate Average Fuel Economy

**CAN** - Control Area Network

**CAS** - Combustion Analysis System

**cEGR** - Cooled EGR

**CO<sub>2</sub>** - Carbon Dioxide

**COV** - Coefficient of Variation

**CKP** - Crankshaft Position Sensor

**CMP** - Camshaft Position Sensor

**CR** - Compression Ratio

**CVS** - constant volume sampling

**deacFC** - Full Continuous Cylinder Deactivation

**deacPD** - Partial Discrete Cylinder Deactivation

**DFCO** - Deceleration Fuel Cut Off

**DI** - Direct Injection

**dur<sub>inj</sub>** - Injector-open during (time)

**ECU** - Engine Control Unit

**EGR** - Exhaust Gas Recirculation

**EGRB** - Exhaust Gas Recirculation with Boosting

**EIVC** - Early Intake Valve Closing

**EPA** - U.S. Environmental Protection Agency

**EVC** - Exhaust Valve Close

**EVO** - Exhaust Valve Open

**FTP** - U.S. Light-duty Federal Test Procedure or City Cycle

**FEAD** - Front End Accessory Drive

**GDI** - Gasoline Direct Injection

**GHG** - Greenhouse Gas

**I/O** - Input/Output

**I4** - Inline 4-cylinder Engine

**IVC** - Intake Valve Close

**IVO** - Intake Valve Open

**HWFET** - U.S. Light-duty Highway Fuel Economy Test or Highway Cycle

**LHV** - Lower Heating Value

**LIVC** - Late Intake Valve Closing

**m** - Regression Slope

**NCAT** - National Center for Advanced Technologies

**NVFEL** - National Vehicle and Fuel Emissions Laboratory

**NVH** - Noise, vibration, harshness

**OBD** - Onboard Diagnostics

**OE** - Original Equipment

**PFI** - Port Fuel Injection

**P<sub>rail</sub>** - High-pressure Fuel Rail Pressure

**q<sub>fuel</sub>** - Injected fuel quantity

**RL** - Road Load

**RPECS** - Rapid Prototyping Electronic Control System

**RPM** - Revolutions per Minute

**SCFM** - Standard Cubic Feet per Minute

**SPCCI** - Spark Controlled Compression Ignition

**SwRI** - Southwest Research Institute

**TDC** - Top Dead Center

**US06** - U.S. Supplemental Federal Test Procedure High-speed/Aggressive Driving Cycle

**V8** - Vee-configured 8-cylinder Engine

**VVT** - Variable Valve Timing

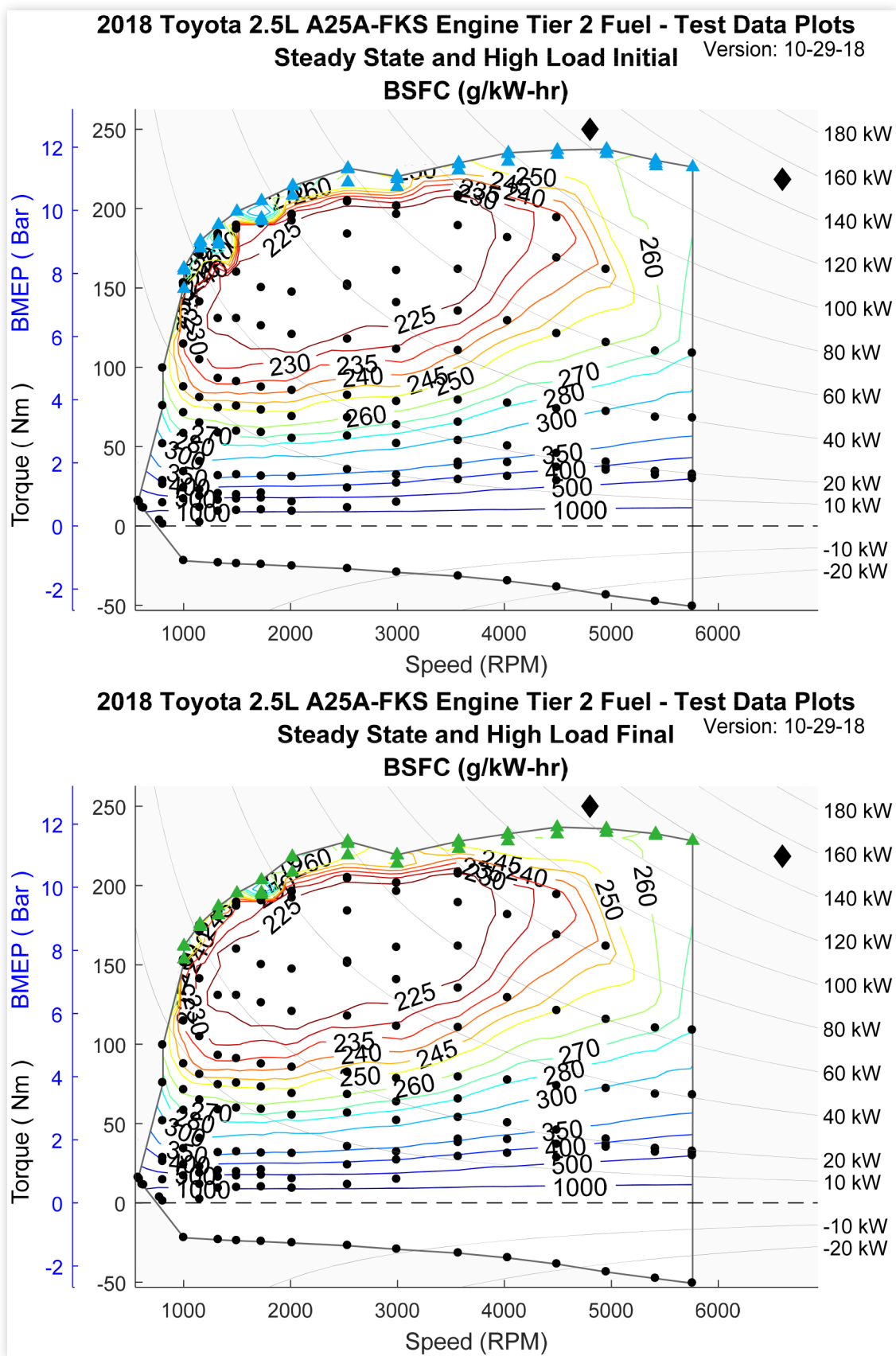
**WOT** - Wide open throttle

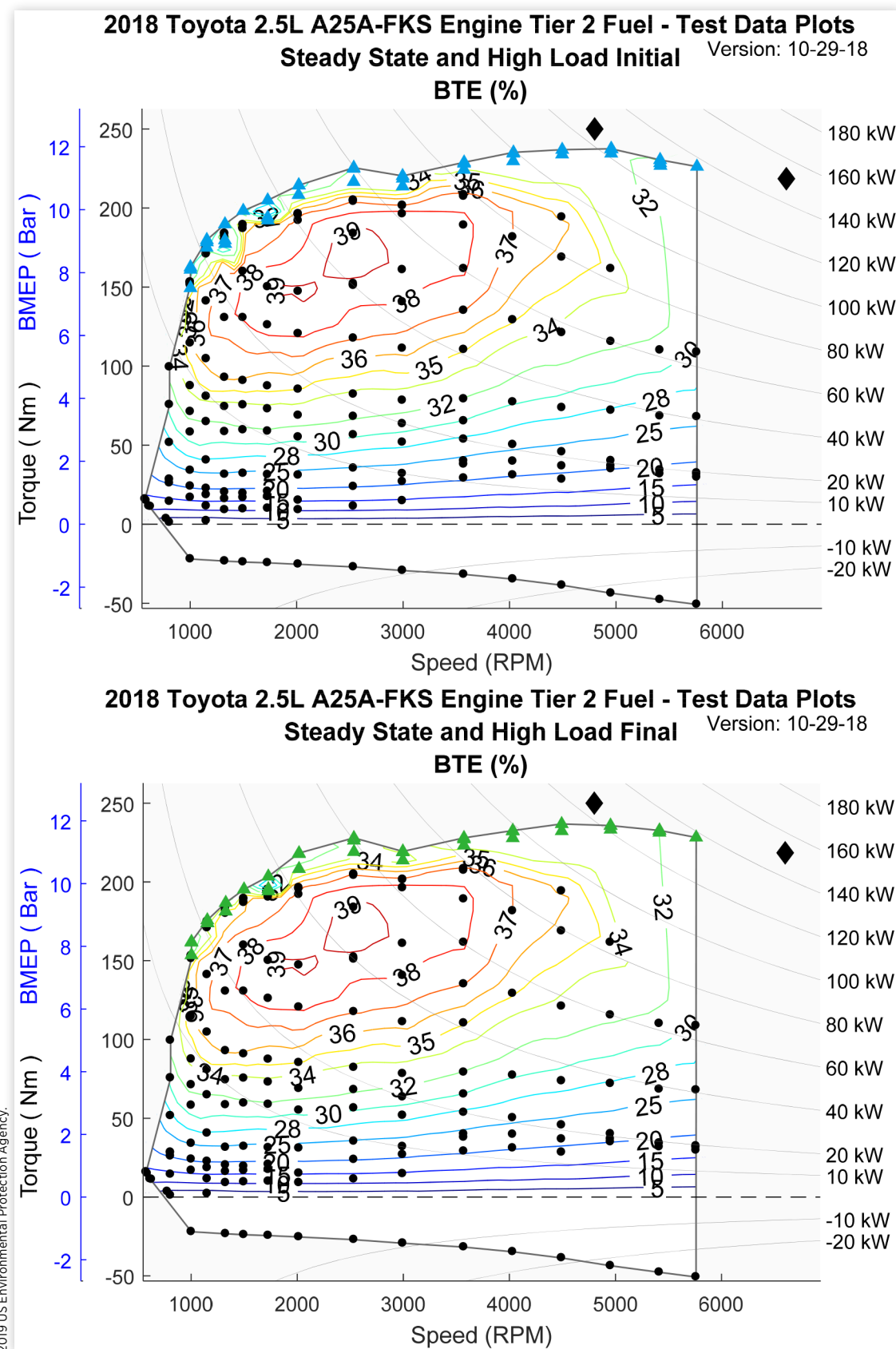
## Appendix

### Benchmarking Plots for the 2018 Toyota 2.5-liter A25A-FKS Engine

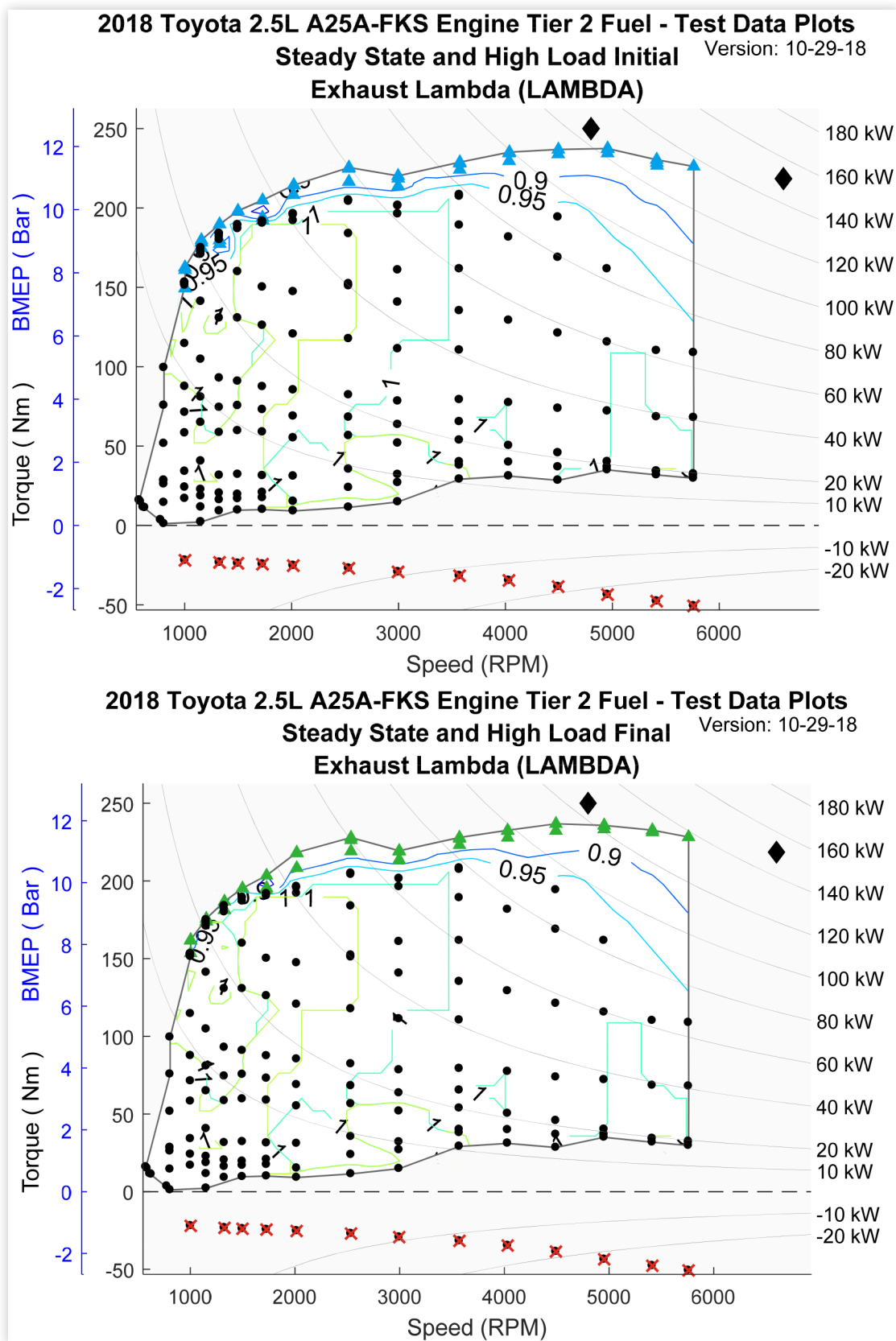
Note: Several of these figures include both "Initial" and "Final" windows of operation to show how measured parameters change in high load region. The initial window is just after torque value is reached and the final value is after several seconds of operation when engine controls stabilize.

1. Figure A1 Steady-State and High Load Initial and Final BSFC maps for the 2018 Toyota 2.5-liter A25A-FKS Engine
2. Figure A2 Steady-State and High Load Initial and Final BTE maps for the 2018 Toyota 2.5-liter A25A-FKS Engine
3. Figure A3 Steady-State and High Load Initial and Final Exhaust Lambda Maps for the 2018 Toyota 2.5-liter A25A-FKS Engine
4. Figure A4 Steady-State and High Load Initial and Final Effective Compression Ratio Maps for the 2018 Toyota 2.5-liter A25A-FKS Engine
5. Figure A5 Steady-State and High Load Initial and Final Exhaust Valve Open Maps for the 2018 Toyota 2.5-liter A25A-FKS Engine
6. Figure A6 Steady-State and High Load Initial and Final Exhaust Valve Close Maps for the 2018 Toyota 2.5-liter A25A-FKS Engine
7. Figure A7 Steady-State and High Load Initial and Final Intake Valve Open Maps for the 2018 Toyota 2.5-liter A25A-FKS Engine
8. Figure A8 Steady-State and High Load Initial and Final Intake Valve Close Maps for the 2018 Toyota 2.5-liter A25A-FKS Engine
9. Figure A9 Steady-State and High Load Initial and Final Atkinson Ratio Maps for the 2018 Toyota 2.5-liter A25A-FKS Engine
10. Figure A10 Steady-State and High Load Initial and Final Spark Timing Maps for the 2018 Toyota 2.5-liter A25A-FKS Engine
11. Figure A11 Steady-State and High Load Initial and Final Valve Overlap Maps for the 2018 Toyota 2.5-liter A25A-FKS Engine
12. Figure A12 Fuel Flow Measurement Maps for the PFI injectors and GDI injectors under steady-state conditions - Tier 2 fuel
13. Figure A13 Complete BSFC and BTE Maps for the 2018 Toyota 2.5-liter A25A-FKS Engine - Tier 2 fuel Figure A5 Steady-State and High Load Initial and Final Exhaust Valve Open Maps for the 2018 Toyota 2.5-liter A25A-FKS Engine  
(Note: phase is measured relative to the VVT actuator parked position)

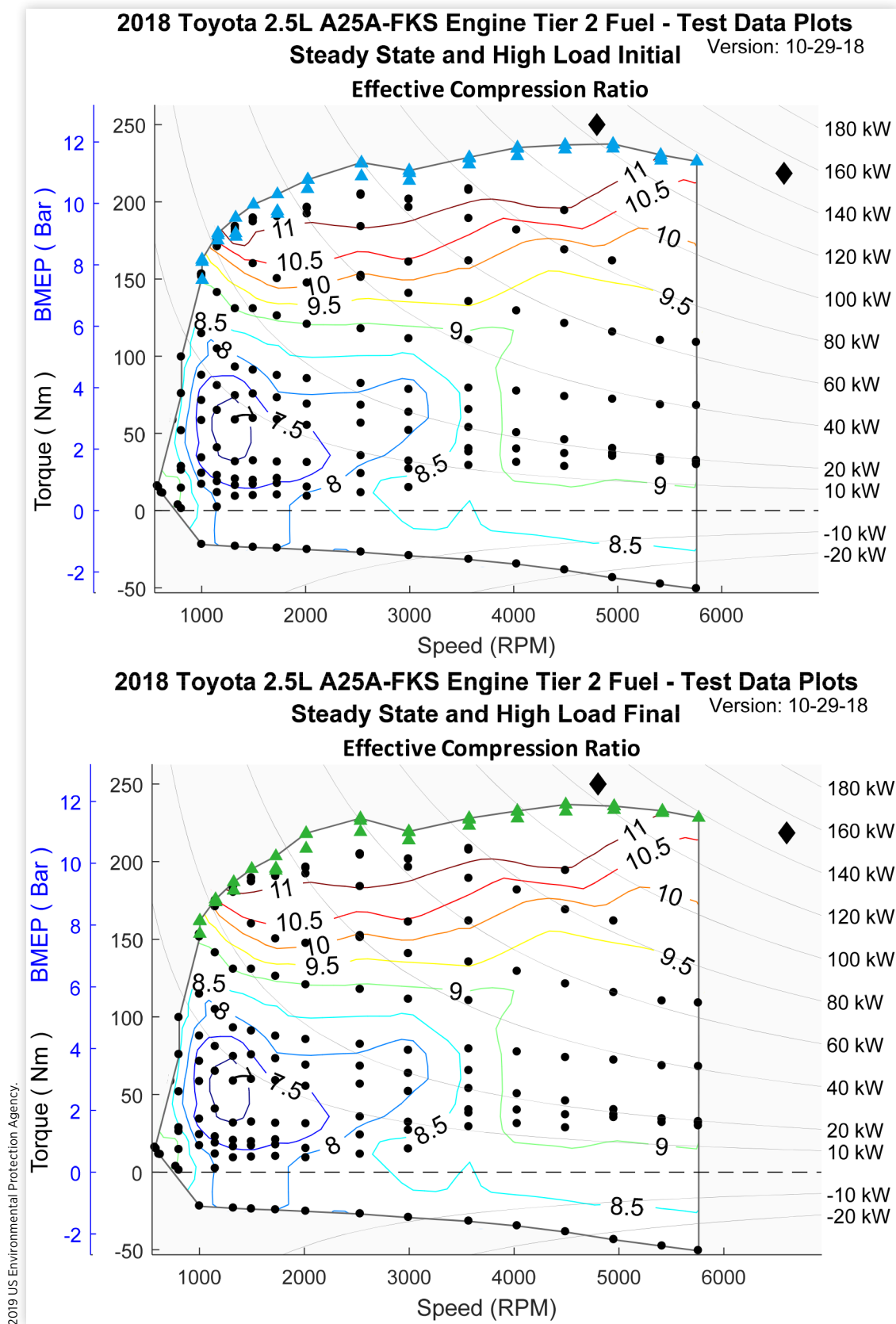
**FIGURE A1** Steady-State and High Load Initial and Final BSFC Maps for the 2018 Toyota 2.5-liter A25A-FKS Engine

**FIGURE A2** Steady-State and High Load Initial and Final BTE Maps for the 2018 Toyota 2.5-liter A25A-FKS Engine

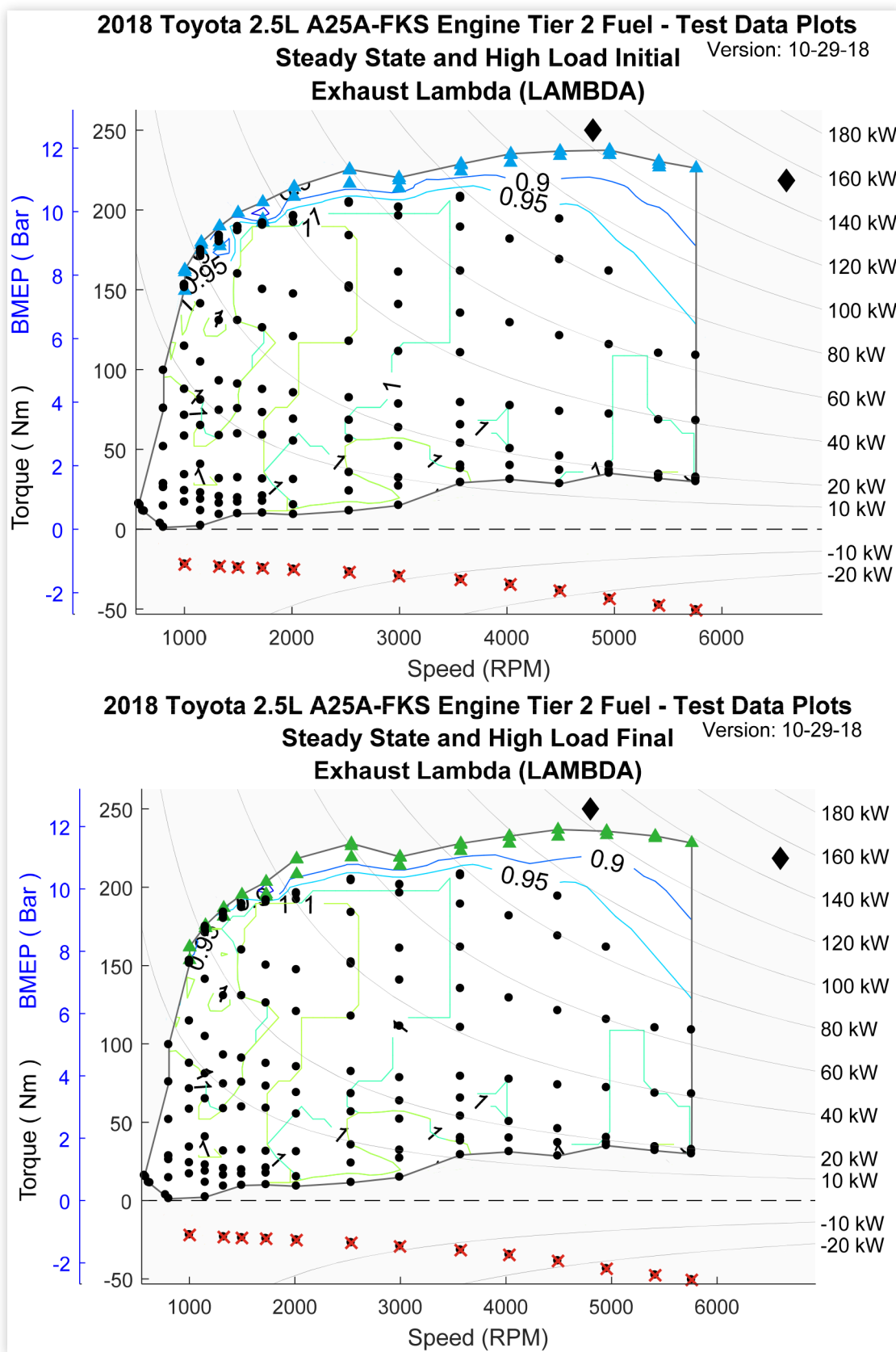
**FIGURE A3** Steady-State and High Load Initial and Final Exhaust Lambda Maps for the 2018 Toyota 2.5-liter A25A-FKS Engine  
(Note: The air-fuel ratio analyzer contains a wideband oxygen sensor which is operated per factory suggested settings.)



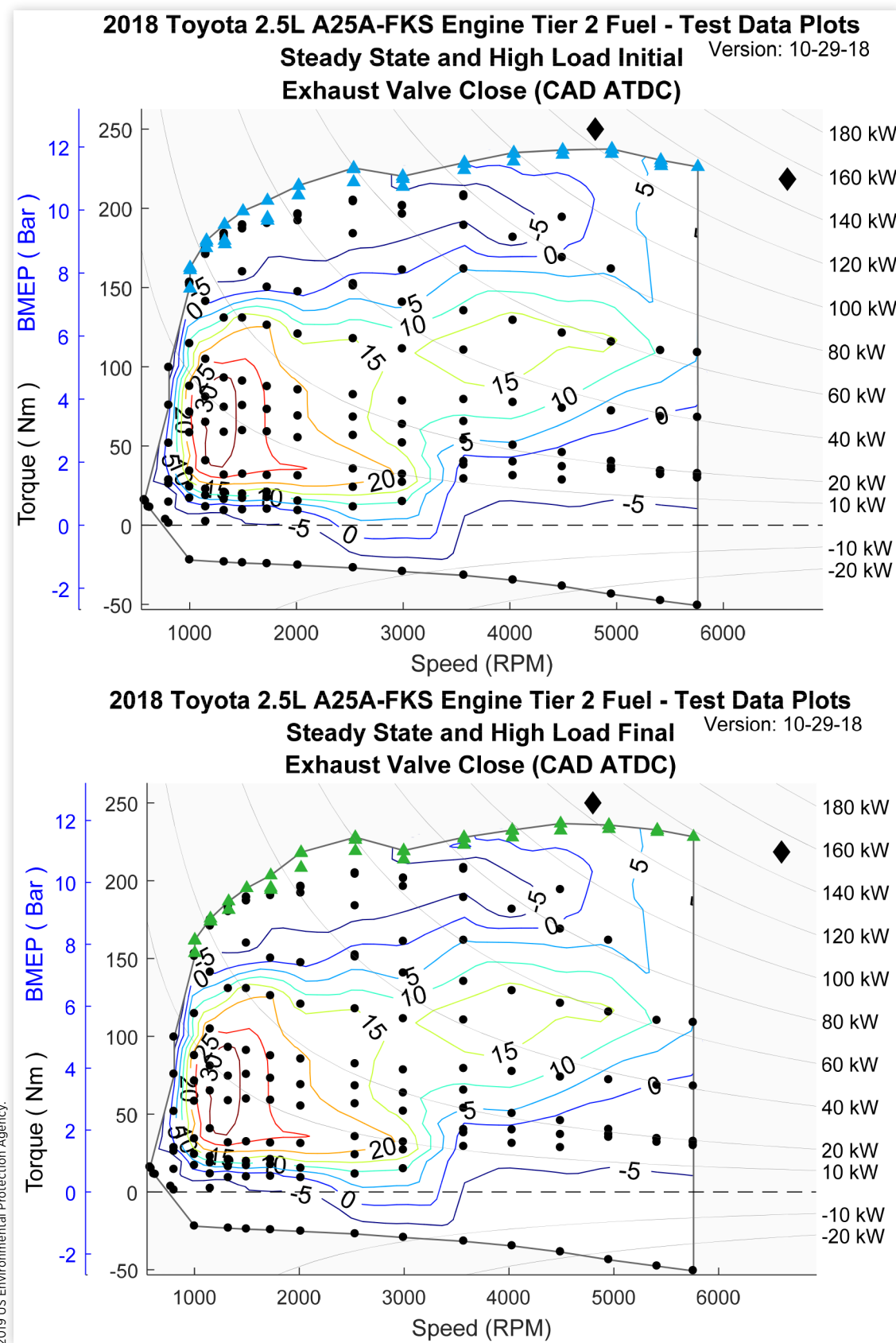
**FIGURE A4** Steady-State and High Load Initial and Final Effective Compression Ratio Maps for the 2018 Toyota 2.5-liter A25A-FKS Engine



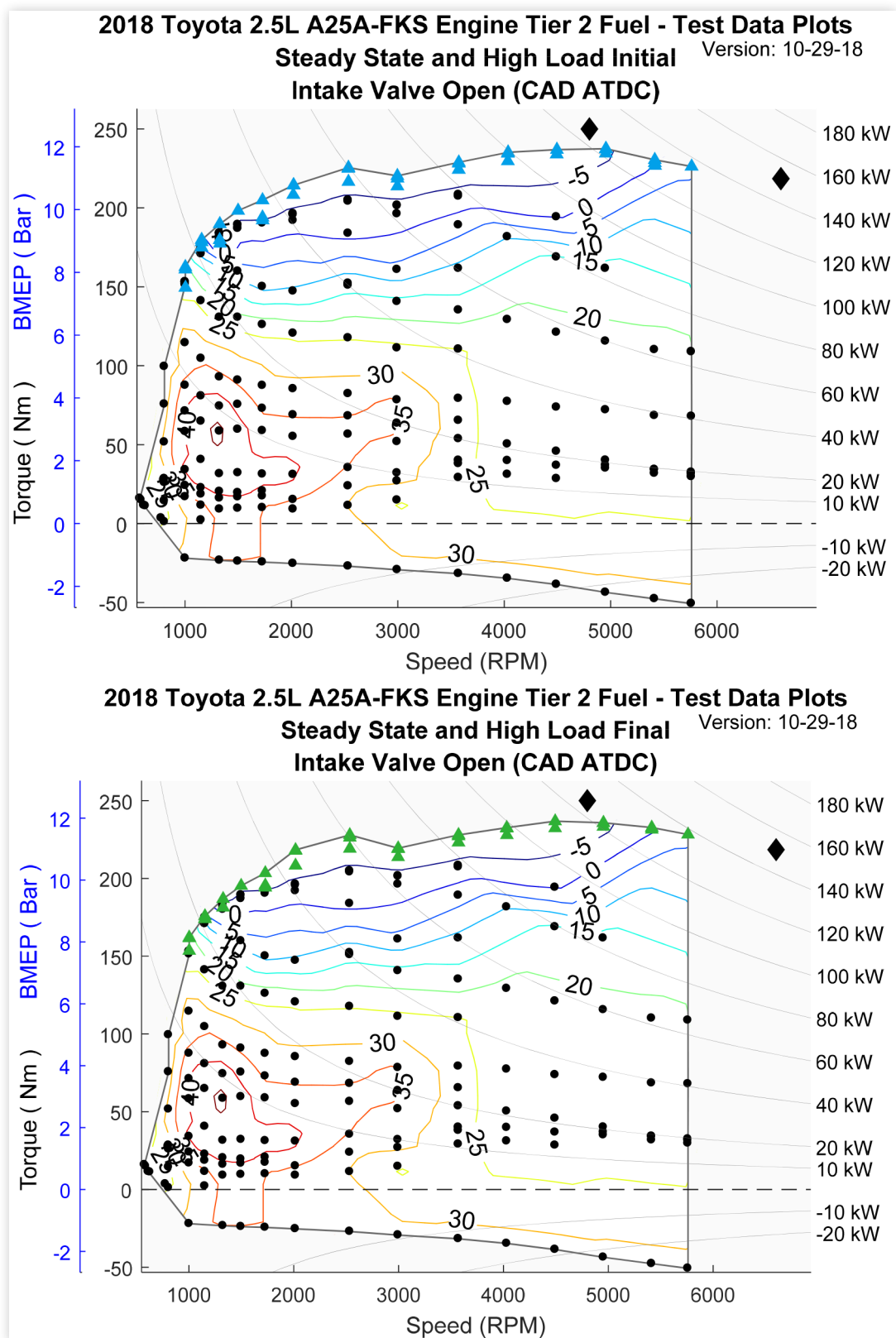
**FIGURE A5** Steady-State and High Load Initial and Final Effective Compression Ratio Maps for the 2018 Toyota 2.5-liter A25A-FKS Engine (Note: event locations are determined at 1mm valve lift)



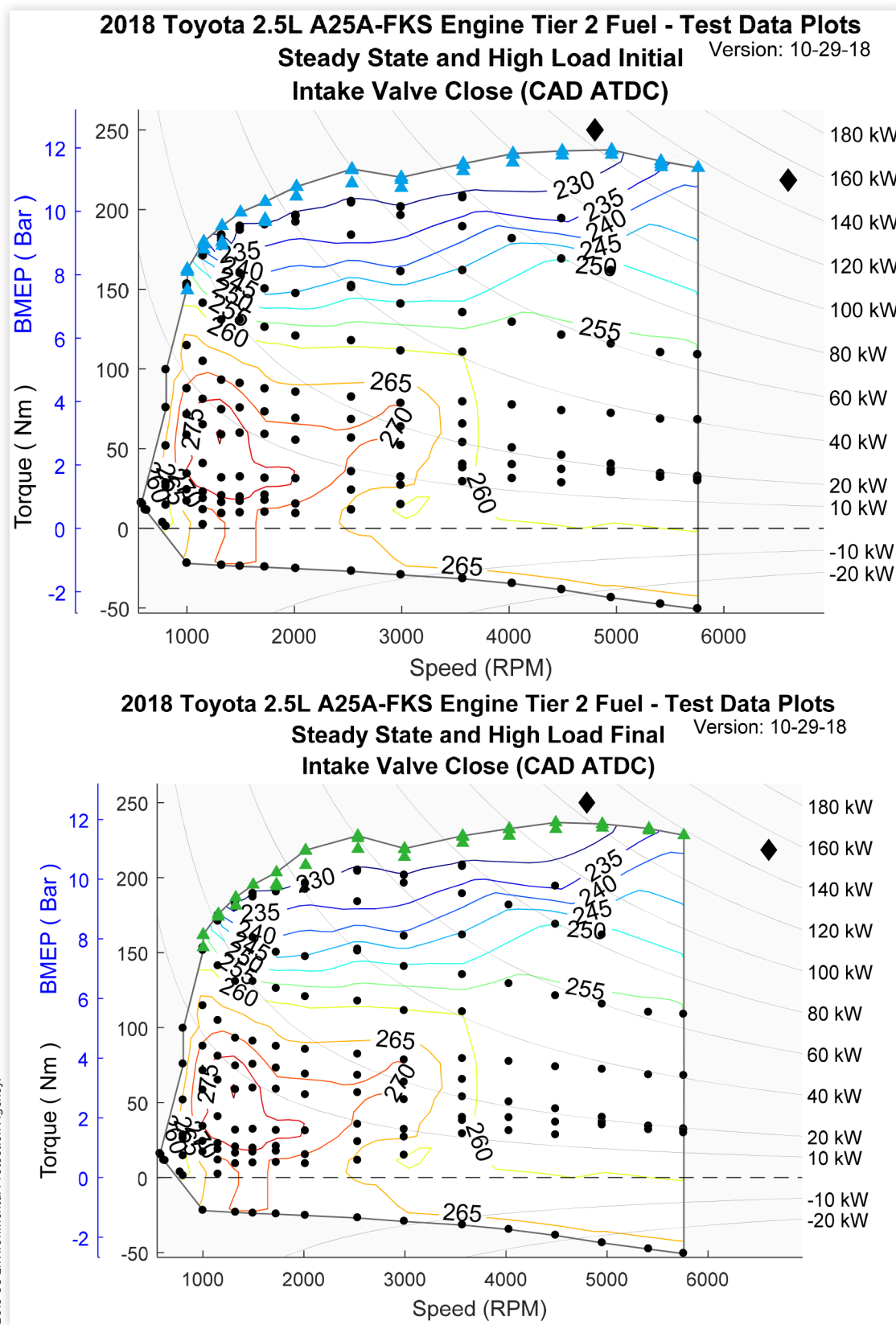
**FIGURE A6** Steady-State and High Load Initial and Final Exhaust Valve Closed Maps for the 2018 Toyota 2.5-liter A25A-FKS Engine (Note: phase is measured relative to the VVT actuator parked position)



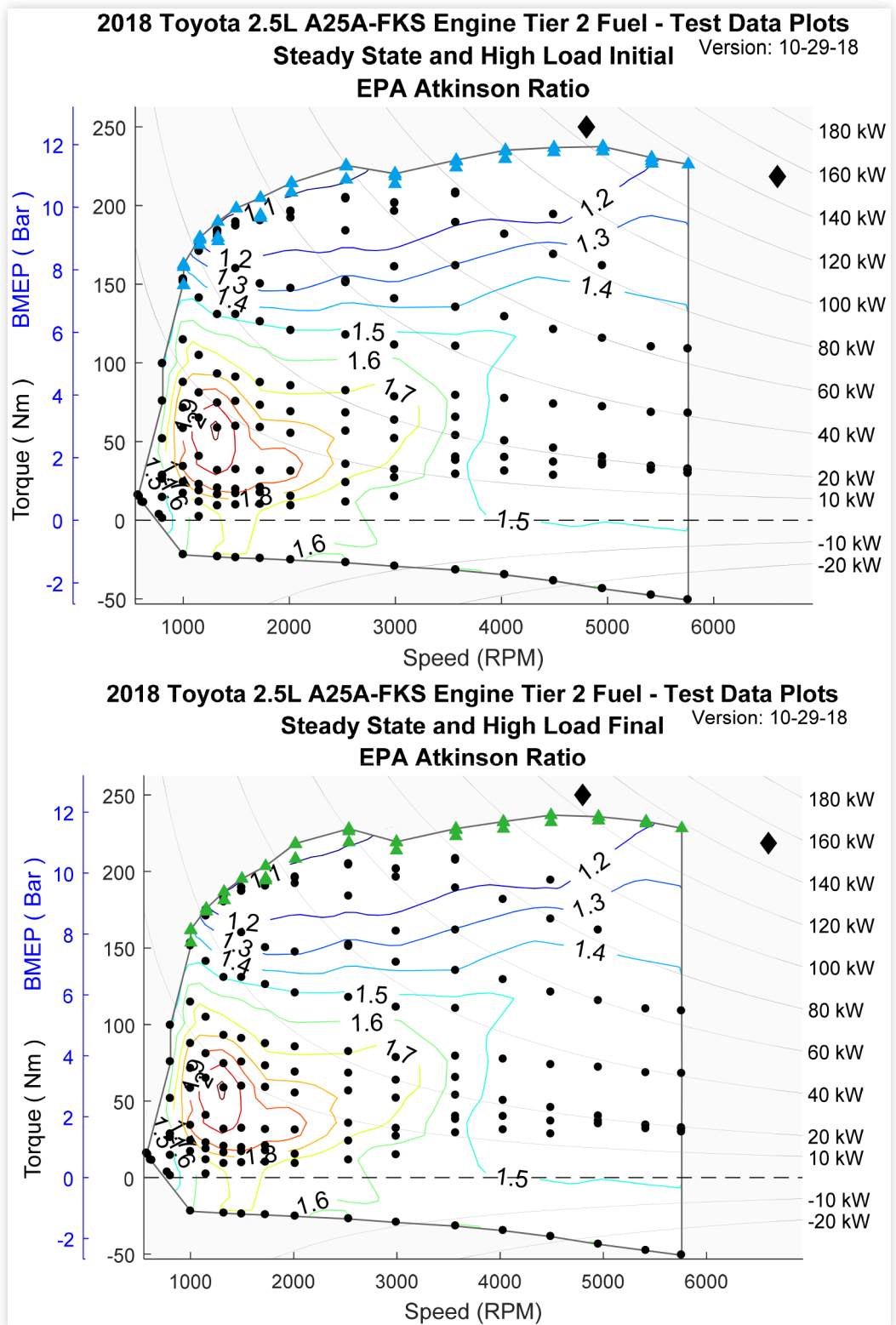
**FIGURE A7** Steady-State and High Load Initial and Final Intake Valve Open Maps for the 2018 Toyota 2.5-liter A25A-FKS Engine  
(Note: phase is measured relative to the VVT actuator parked position)



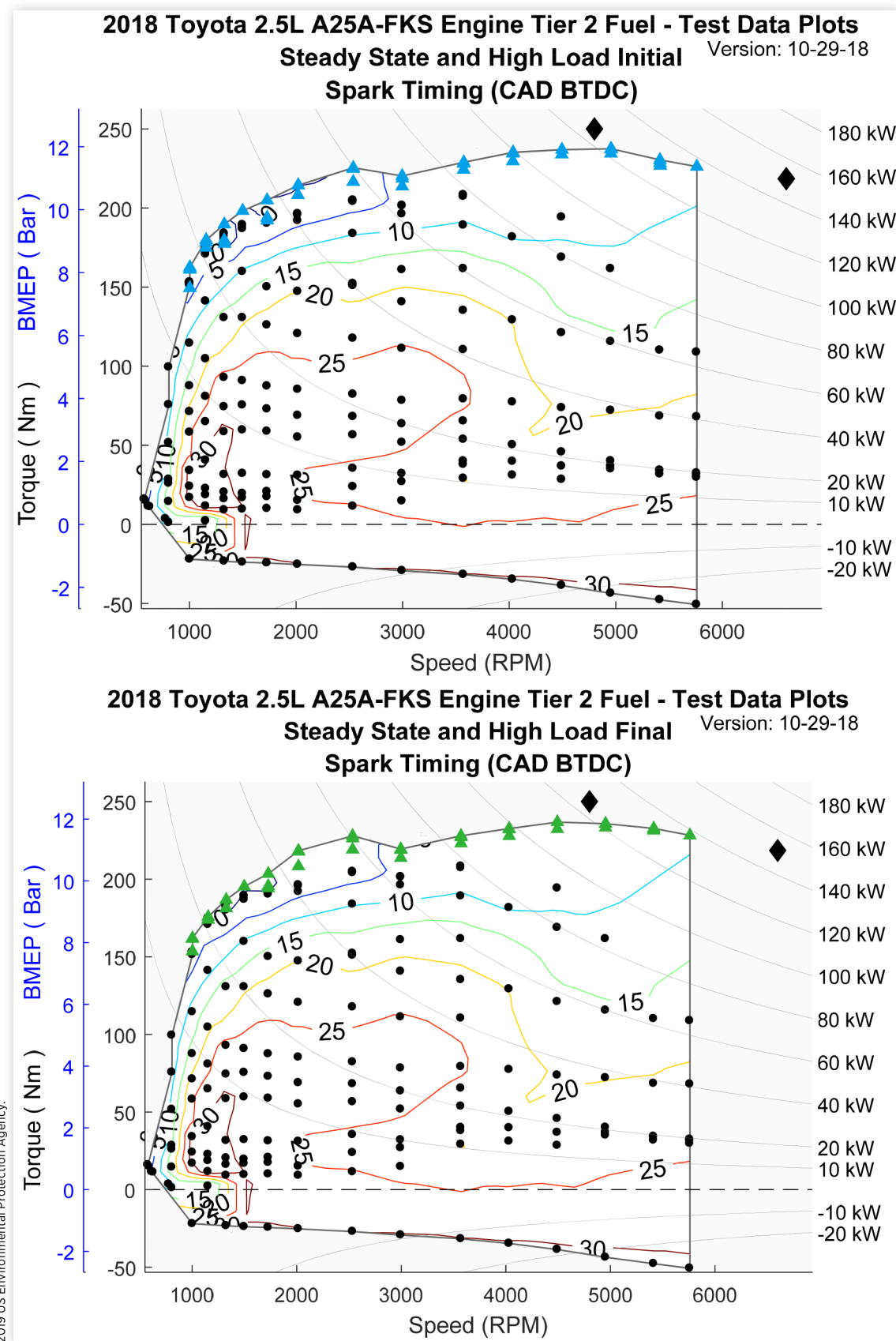
**FIGURE A8** Steady-State and High Load Initial and Final Intake Valve Closed Maps for the 2018 Toyota 2.5-liter A25A-FKS Engine (Note: phase is measured relative to the VVT actuator parked position)



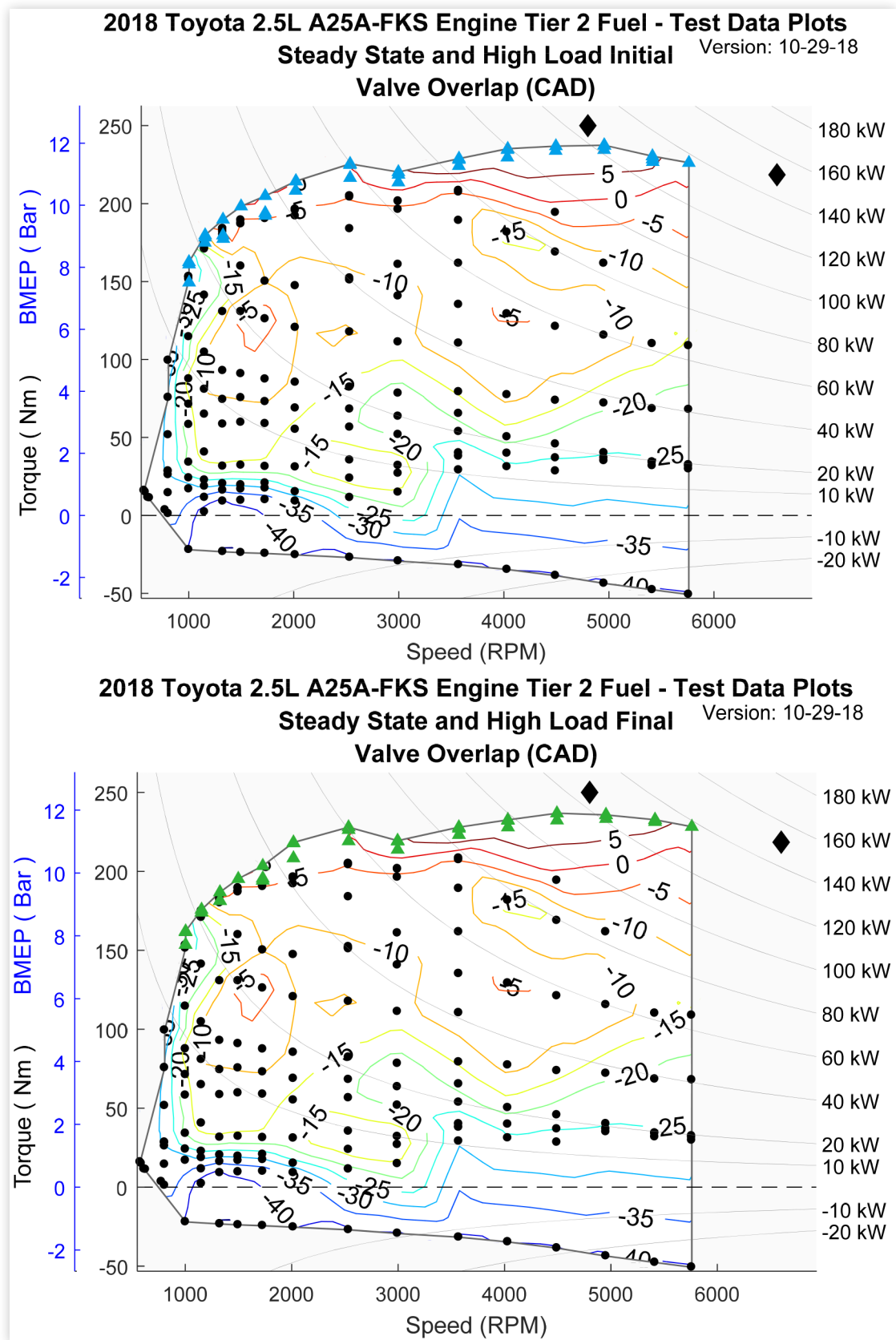
**FIGURE A9** Steady-State and High Load Initial and Final Atkinson Ratio Maps for the 2018 Toyota 2.5-liter A25A-FKS Engine (For this study, the Atkinson Ratio is the ratio of effective expansion ratio to effective compression ratio where the extremity of each stroke is determined by the location corresponding to 1mm of valve lift.)



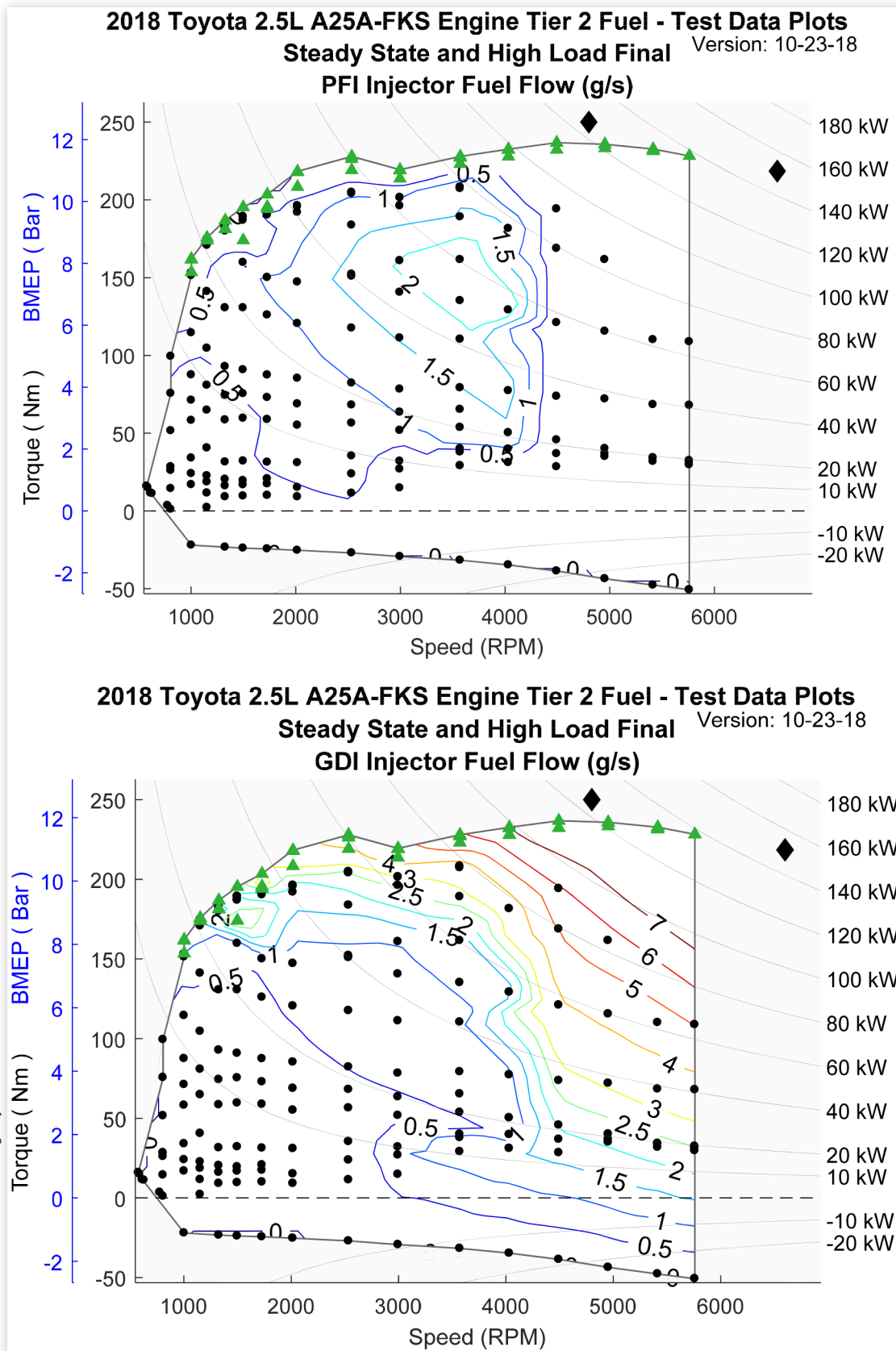
2019 US Environmental Protection Agency.

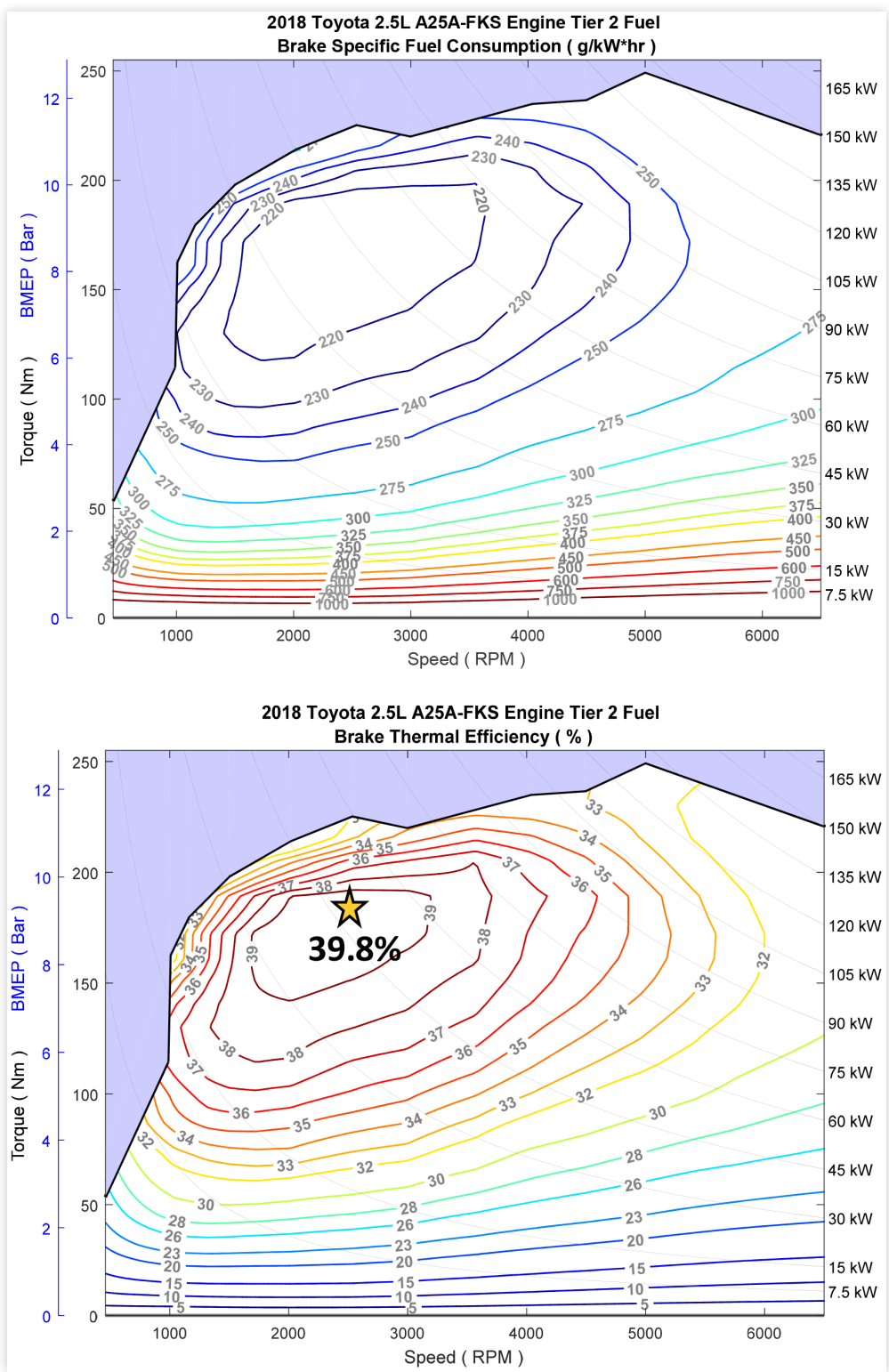
**FIGURE A10** Steady-State and High Load Initial and Final Spark Timing Maps for the 2018 Toyota 2.5-liter A25A-FKS Engine

**FIGURE A11** Steady-State and High Load Initial and Final Valve Overlap Maps for the 2018 Toyota 2.5-liter A25A-FKS Engine  
 (Note: valve opening and closing events are defined by 1 mm valve lift)



**FIGURE A12** Fuel flow measurement map (g/s) for the PFI injectors (top) and the GDI injectors (bottom) under steady-state conditions



**FIGURE A13** Complete BSFC and BTE Maps for the 2018 Toyota 2.5-liter A25A-FKS Engine - Tier 2 fuel

2019 US Environmental Protection Agency.

2019 US Environmental Protection Agency. This is the work of a Government and is not subject to copyright protection. Foreign copyrights may apply. The Government under which this work was written assumes no liability or responsibility for the contents of this work or the use of this work, nor is it endorsing any manufacturers, products, or services cited herein and any trade name that may appear in the work has been included only because it has been deemed essential to the contents of the work.

Positions and opinions advanced in this work are those of the author(s) and not necessarily those of SAE International. Responsibility for the content of the work lies solely with the author(s).